Food Bioscience 80 (2026) 108934

Contents lists available at ScienceDirect

Food Bioscience

journal homepage: www.elsevier.com/locate/fbio

Laboratory scale-up of ultrasound-assisted extraction of phenolic compounds from tropical fruit peel by-products: modelling, on-line process monitoring, and product characterization

Luis Condezo-Hoyos [a,b,*], Narda Velasco-Salazar [c], Lilian Toribio-Lopez [c], Paola Cortés-Avendaño [a,b], Julio Vidaurre-Ruiz [c], Paulo Torres-Mayanga [a,b], Jukka-Pekka Suomela [d], Baoru Yang [d], Ye Tian [d,**]

[a] Innovative Technology, Food and Health Research Group, Facultad de Industrias Alimentarias, Universidad Nacional Agraria La Molina, Av. La Molina s/n, Lima, Peru
[b] Instituto de Investigación de Bioquímica y Biología Molecular, Universidad Nacional Agraria La Molina, Av. La Molina s/n, Lima, Peru
[c] Facultad de Industrias Alimentarias, Universidad Nacional Agraria La Molina, Av. La Molina s/n, Lima, Peru
[d] Food Sciences, Department of Life Technologies, Faculty of Technology, University of Turku, FI-20014, Turku, Finland

ARTICLE INFO

Keywords:
Agri-food byproducts
Byproduct revalorization
High intensity ultrasound
Phenolic compounds extraction
Laboratory scale-up of ultrasound-assisted extraction

ABSTRACT

This study sought to extract phenolic compounds (PC) from the byproduct peels of starfruit (AC-p), camu camu (MD-p), and elderberry (SP-p) through laboratory-scale ultrasound-assisted extraction (UAE). The UAE process used different levels of acoustic energy density (AED = 25–100 J/mL) and nominal amplitude. The particle size and distribution AC-p, MD-p, and SP-p were characterized. The total phenolic content (TPC) extracted via small-scale laboratory UAE using an S24d7 sonotrode (UAE-S24d7) exhibited no significant variation at amplitudes of 49 and 63 μm, achieving a maximum value at 25 J/mL, as confirmed by Fourier-transform infrared (FT-IR) spectroscopy. The TPC and AED for UAE-S24d7 were modeled using a diffusion-based mathematical approach, and the ultrasonic net power of UAE was observed in the order of AC-p > MD-p > SP-p, which correlates with particle size distribution and temperature increase, as confirmed by thermal analysis. The TPC of extracts obtained through laboratory-scale UAE (25 J/mL and 49 μm) using an S24d14 sonotrode (UAE-S24d14) did not differ statistically from those obtained using an S24d7 sonotrode (UAE-S24d7). The PC were identified using liquid chromatography tandem mass spectrometry in AC-p, MD-p, and SP-p at UAE-S24d14, including flavonols, proanthocyanidins, hydroxycinnamic acids, anthocyanins, flavan-3-ols, flavone, and hydroxybenzoic acid derivatives. The laboratory scale-up extracts also demonstrated antioxidant capacity, assessed by DPPH (138.1-307.6 μmol TE/g), ABTS (154.2-466.7 μmol TE/g), ORAC (483.1-882.9 μmol TE/g), and superoxide anion (413.2-4964.62 μmol TE/g). In conclusion, AED and nominal amplitude facilitate the laboratory scaling-up of UAE for the valorization of food by-products.

1. Introduction

Ultrasound-assisted extraction (UAE) is recognized as a sustainable technology that employs ultrasonic waves (20-100 kHz) to enhance the efficiency of extracting bioactive compounds from food matrices, botanical vegetables, and pharmaceutical formulations. This enhancement is attributed to the mechanical energy generated by cavitation, which involves the implosion of numerous vacuum bubbles, producing powerful shearing forces that propagate as microjets (speeds ≈ 280 m/s) and shock waves (5000 °C, 200 MPa). These forces increase the surface area by reducing particle size through cell lysis, facilitating the penetration of the extractant, and improving diffusion and mass transfer (Bello et al., 2025; Boateng & Clark, 2024; Gil-Martin et al., 2022; Shahbaz, Riaz, Momal, Rasool, Naeem, Raza, et al., 2025). These forces increase the surface area by reducing particle size through cell lysis, facilitating the penetration of the extractant, and improving diffusion

* Corresponding author. Innovative Technology, Food and Health Research Group, Facultad de Industrias Alimentarias, Universidad Nacional Agraria La Molina, Av. La Molina s/n, Lima, Peru.
** Corresponding author. Food Sciences, Department of Life Technologies, Faculty of Technology, University of Turku, Turku, Finland.
E-mail addresses: lcondezo@lamolina.edu.pe (L. Condezo-Hoyos), yetia@utu.fi (Y. Tian).

https://doi.org/10.1016/j.fbio.2026.108934
Received 10 March 2026; Received in revised form 1 April 2026; Accepted 15 April 2026
Available online 16 April 2026

and mass transfer (Bello et al., 2025; Boateng & Clark, 2024; Gil-Martin et al., 2022; Shahbaz et al., 2025). Over the past decade, extensive research has explored UAE as a straightforward, environmentally friendly, and cost-effective alternative to conventional extraction methods for various agri-food wastes, contributing to their revalorization and advancing a circular economy in the food industry (Avdović, Antonijević, Simijonović, Grujović, Marković, Milenković, et al., 2025; Carciochi et al., 2017; Kumar et al., 2021; Noor et al., 2024; Pandey et al., 2025; Shahbaz et al., 2025). To date, the UAE has been primarily used to extract antioxidative components (such as phenolic compounds), proteins, and pectin from agri-food byproducts (Fig. 1).

UAE systems are available in different configurations, such as ultrasonic baths with transducers and ultrasonic horns or probes, though ultrasonic bath methods tend to be less consistent than those using probes (Boateng & Clark, 2024). The effectiveness of UAE is affected by factors like the type of solvent, the ratio of solvent to solid, temperature, and pH, along with ultrasound-specific factors such as acoustic energy density (AED), ultrasonic intensity, ultrasound power, amplitude, frequency, and whether the operation is pulsed or continuous, all of which were optimized using response surface methodology (Fig. 1). While there has been extensive research on extracting phenolic compounds from agri-food byproducts using UAE, only a few studies have focused on scaling up the process (Gogate et al., 2011). The lack of this crucial aspect in the development of ultrasound technology is due to the absence of standardized design and scale-up strategies. Many studies have utilized ultrasound variables such as time, nominal ultrasound power, and amplitude percentage to optimize UAE. However, ultrasound time is not a scale-up parameter since it relies on ultrasound power, and the actual energy applied to the sample varies with the ultrasound system. AED is an intensive parameter that remains constant regardless of scale, making it possible to scale any ultrasonic process using this parameter (Natolino & Celotti, 2022; Patist & Bates, 2011). Additionally, the percentage of ultrasound amplitude does not indicate the nominal amplitude; it is well-known that values exceeding 63 μm are not suitable for scale-up processes because the probe may break (Hielscher, 2012).

To fill up this technical gap, the present research aimed to develop a laboratory-level scale-up UAE approach to extract phenolic compounds from tropical fruit peel by-products. As the novelty of our present research, the scale-up method was optimized based on AED, nominal amplitude, and reactor geometry. The peels of starfruit (*Averrhoa carambola*), camu camu (*Myrciaria dubia* (H.B.K) McVaugh) and elderberry (*Sambucus peruviana*) were selected and first studied with particle size distribution analysis. The UAE was modeled by monitoring key ultrasound parameters and total content of phenolic compounds. The extracts obtained from scale-up UAE extraction were further investigated. Their phenolic profiles were characterized using liquid chromatography tandem mass spectrometry. The antioxidative capacities of which were also measured using assays based on the single electron transfer (SET) and hydrogen atom transfer (HAT) mixed and HAT mechanisms.

2. Materials and methods

2.1. Raw material

Ripe starfruit (*Averrhoa carambola*) and camu camu (*Myrciaria dubia* (H.B.K) McVaugh) fruits were procured from the Santa Anita market in Lima, Perú, while elderberry (*Sambucus peruviana*) was obtained from Abancay in Apurimac, Perú. The fruits underwent a process of washing and disinfection, followed by the removal of peels through squeezing. The peels from starfruit (AC-p), camu camu (MD-p), and elderberry (SP-p) were subjected to drying for 18 h at −55 °C using an Alpha freeze dryer (Christ, Germany). Post-drying, the peels were ground using a Retsch GM 200 grindomix knife mill (IKA, Germany) and sieved through mesh sizes 18 and 20 (USA Standard ASTM E11). The processed peels were then packed in laminated bags and stored at −20 °C.

2.2. Chemicals

2,2-diphenyl-1-picrylhydrazyl (DPPH), 2,2′-azinobis-(−3-ethylbenzthiazoline-6-suphonate) (ABTS), Fast Blue B Salt, Folin-Ciocalteu, 2,4,6-Tris(2-pyridyl)-triazine (TPTZ), fluorescein (FL), 2,2′-Azobis(2-methylpropionamidine) dihydrochloride (AAPH), dibasic potassium

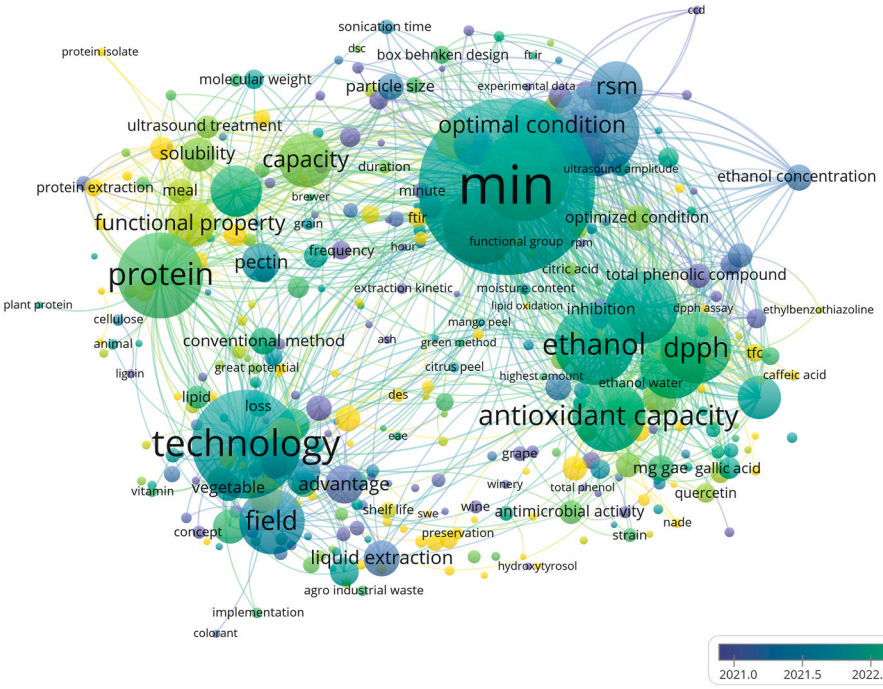

Fig. 1. VOSViewer bibliometric analysis of ultrasound-assisted extraction of by-products. Published papers were downloaded from Scopus Database using the following keywords (Ultrasound OR ultrasound-assisted) AND (extraction) AND (by-products).

phosphate, ethanol, gallic acid, hydrochloric acid, methanol, monobasic potassium phosphate, potassium persulfate, sodium hydroxide and Tris base were acquired from Sigma-Aldrich Chemical Co. (St. Louis, MO, USA). (±)-6-Hydroxy-2,5,7,8-tetramethylchromane-2-carboxylic acid (Trolox) was purchased from EMD Millipore (Billerica, MA, USA).

Reference standards of cyanidin 3-*O*-galactoside, cyanidin 3-*O*-glucoside, cyanidin, peonidin, myricetin 3-*O*-galactoside, myricetin 3-*O*-glucoside, myricetin, kaempferol 3-*O*-glucoside, quercetin 3-*O*-galactoside, quercetin 3-*O*-glucoside, quercetin, isorhamnetin 3-*O*-rutinoside, (+)-catechin, (−)-epicatechin, and procyanidin B2 were purchased from Extrasynthese (Genay, France). Standards of ellagic acid, caffeic acid, 3-*O*-caffeoylquinic acid, 4-*O*-caffeoylquinic acid, and 5-*O*-caffeoylquinic acid were purchased from Sigma-Aldrich Chemical Co. (St. Louis, MO, USA). The solvents of LC and MS grade (methanol, formic acid, ethyl acetate, and acetonitrile) were purchased from Honeywell International Inc. (Charlotte, NC, USA).

2.3. Characterization of Andean and tropical fruit peels

2.3.1. Particle size and distribution

A particle sight 3D dynamic image analyzer (Micromeritics Instrument Corp., GA, USA) was employed to assess the shape and particle size distribution of the ground AC-p, MD-p, and SP-p. To ensure adequate particle individualization, each 0.5 fruit peel powder was suspended and stirred at 350 rpm. The suspension was subsequently pumped through a thin flow cell situated in the optical path, with a high-resolution CCD camera and telecentric optics utilized to maintain full focus (Ulusoy & Yekeler, 2014). Particle Insight software (Micromeritics Instrument Corp., GA, USA) was employed to quantify the equivalent circular area diameter (ECAD), and equivalent circular perimeter diameter (ECPD) in triplicate.

2.3.2. FT-IR spectra

The ground AC-p, MD-p, and SP-p infrared spectra were measured in triplicate in the 400–4000 cm^{-1} range using a Spectrum Two FT-IR spectrometer (PerkinElmer, USA) in attenuated total reflection (ATR) mode with 32 scans and a resolution of 4 cm^{-1} (Condezo-Hoyos et al., 2024).

2.4. UAE of phenolic compounds from fruit peels at a small-scale laboratory: parameters, mathematical modelling, and monitoring

2.4.1. UAE parameters and mathematical modelling

Ground AC-p (2 g), MD-p (2 g), and SP-p (1 g) were suspended in 20 mL (V_o) of an ethanol aqueous solution (30% v/v). The UAE at small-scale laboratory system of phenolic compounds was conducted using a 24 kHz low-frequency system, specifically the UP400St Ultrasonic Processors equipped with an S24d7 sonotrode (Hielscher Ultrasonics, Germany), and a reactor maintained at 15 °C through cold water recirculation ($D_0 = 7$ mm, $D_R = 26$ mm, $h_0 = 23$ mm, Fig. 2A). The small-scale laboratory system was performed at amplitudes of 49 μm and 63 μm, with acoustic specific energies (AED) of 25, 50, 75, 100, and 125 J/mL. The amplitudes were derived from standard sonotrode data, with the equivalence of 100% amplitude equating to 164 μm, as provided by the manufacturer in the operating manual. The acoustic specific energy (AED) was determined by automatically measuring the power of the UP400St Ultrasonic Processors using an integrated potentiometer, following prior calibration of the equipment in air to obviate the need for calorimetric analysis.

The experimental quantification of phenolic compounds under varying ultrasound conditions was modeled using a modified diffusion model derived from Fick's second law, as previously outlined by López et al. (2023). The modifications to this model involved the application of AED (J/mL) as suggested by Natolino and Celotti (2022) (Eq. (1)).

$$C = C_d\left(1 - e^{-kAED}\right) \quad (1)$$

Where C is the concentration of total phenolic compounds at AED, C_d is the final concentration of total polyphenols and k is the apparent first-order rate constant of extraction.

2.4.2. UAE process monitoring

The net power (W), applied energy (J), and temperature (°C) were monitored during the process using the UP400St Ultrasonic Processors data acquisition system (Hielscher Ultrasonics, Germany). Additionally, thermal analysis was conducted in quadruplicate for each of AC-p, MD-p, and SP-p under the sonication conditions (amplitude and AED) specified for each sample in the mathematical modelling section. The

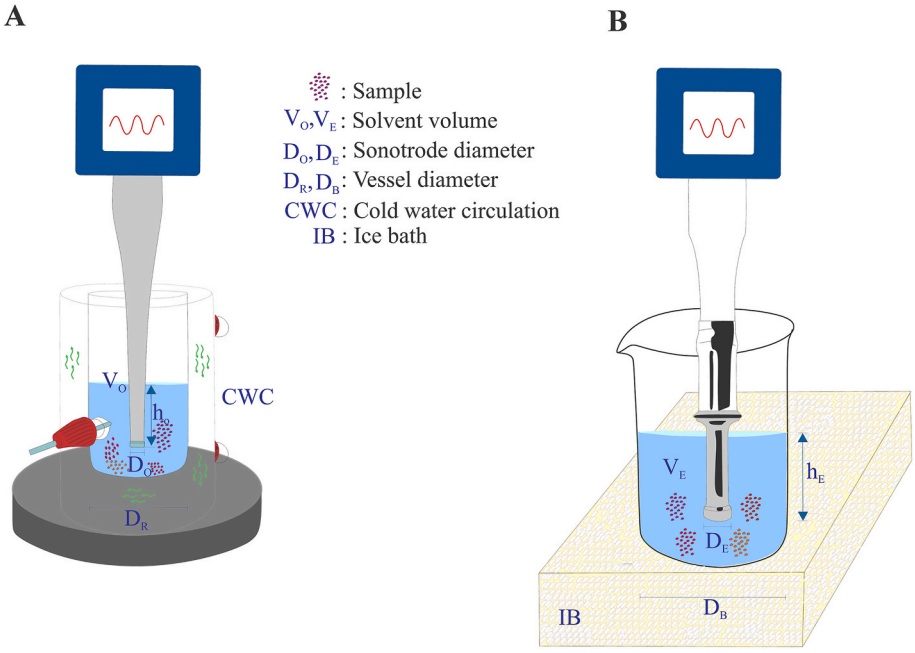

Fig. 2. Ultrasound system to phenolic extraction from peels of starfruit (AC-p), camu camu (MD-p), and elderberry (SP-p). Small-scale (A) and scale-up (B) laboratory systems.

cooling jacket surrounding the vessel was intentionally excluded from the analysis to ensure that the assessment solely reflected the thermal behavior induced by sonication. AC-p, MD-p, and SP-p were suspended in an ethanol aqueous solution of 30% v/v at the same solvent/solid ratio as in section 2.4.1 and optimal ultrasound parameters of AED = 25 J/mL and nominal amplitude = 49 μm. A high-resolution thermal imaging camera, the TarisIR mini-600 (Infratech GmbH, Germany), was consistently positioned at a fixed and uniform distance during all experimental trials. Thermal images were continuously recorded for a duration corresponding to the input AED of ultrasound. To analyze the spatial evolution of surface heating, thermal frames were extracted and examined every second from the Region of Interest (ROI) using IRBIS 3 Professional software (InfraTec GmbH, Germany). The central region of the extraction vessel was identified as ROI due to the observed maximum exposure to ultrasonic energy. The Thermal Spatial Complexity Index (TSCI) was employed to quantify the spatial complexity of the temperature distribution within the ROI (Eq. (2)). TSCI is a novel metric that integrates the mean, variance, and Shannon entropy of the temperature, and it is proposed to characterize the spatial complexity of the thermal profiles during ultrasound treatments (Eq. (2) and Eq. (3)). Individual values were utilized to analyze the thermal images (Rojas-Lima et al., 2021).

$$TSCI = \frac{\sigma^2 H}{\mu} \tag{2}$$

$$\sigma^2 = \frac{1}{N}\sum_{i=1}^{N}(T_i - \mu)\, H = -\sum_{i=1}^{M} p_k \, Log\, 2\, p_k \, \mu = \frac{1}{N}\sum_{i=1}^{N} T_i \tag{3}$$

Where σ^2 is the temperature variance, H is the Shannon entropy of the temperature distribution, and μ is the mean temperature, N is the total number of pixels, T_i is the temperature of pixel *i*, M is the number of bins (discretized temperature intervals), and pk is the probability that a pixel falls within bin *k* (calculated as the relative frequency).

Once the TSCI was calculated from the thermal profiles of each ROI, its temporal evolution was modeled using the sigmoidal dose-response function (Eq. (4)). This function enabled the description of typical saturation behavior observed in nonlinear thermal accumulation processes, such as those induced by ultrasound treatments. The fitting procedure was performed in Python using the curve fit function (scipy. optimize) within a Google Colab environment; the source code is available in the Supplementary Material 1. The equation used was as follows:

$$y = y_0 + \frac{(y_{max} - y_0)}{1 + 10^{(LogEC50 - x)HillSlope}} \tag{4}$$

Where y is the value of TSCI as a function of time x, y_0 is the initial TSCI value when x = 0, y_{max} is the maximum TSCI value reached at saturation, LogEC50 is the value of x at which 50% of the total TSCI increase is achieved and HillSlope is the steepness of the curve.

2.5. UAE of phenolic compounds from fruit peels: Laboratory scale up

Ground AC-p (25 g), MD-p (25 g), and SP-p (12.5 g) were subjected to sonication using a low-frequency 24 kHz UP400St Ultrasonic Processor system, equipped with an S24d14D sonotrode (Hielscher Ultrasonics, Germany). The samples were combined with 250 mL (V_E) of a 30% v/v ethanol aqueous solution, and extraction was conducted utilizing the optimal amplitude and AED for each by-product. The sonotrode was centrally positioned 1.5 cm from the base of the 7.5 cm diameter vessel, with the sample covering the initial 4.5 cm from the base of the sonotrode. All sonication extractions were performed with the samples placed in an ice bath to ensure the temperature did not exceed 30 °C (D_E = 14 mm, D_E = 75 mm, h_E = 44 mm, Fig. 2B). The net power (W) and applied energy (J) were monitored using an UP400St ultrasonic processor (Hielscher Ultrasonics, Germany). The extracts obtained from AC-p, MD-p, and SP-p were concentrated using a rotavapor RV 10 (IKA, Germany) at temperatures of 120 °C, 80 °C, and 50 °C, respectively. Subsequently, the samples were subjected to drying in an Alpha freeze dryer (Martin Christ, Germany) for 24 h at −60 °C and 0.020 mbar. The lyophilized samples (AC-p-Lyo, MD-p-Lyo, and SP-p-Lyo) were stored at −80 °C until further analysis.

2.6. Characterization of extracts from fruit peel obtained by UAE

2.6.1. Total phenolic content (TPC)

2.6.1.1. Rapid Folin-Ciocalteu assay. The TPC was determined in triplicate utilizing the rapid and miniaturized Folin-Ciocalteu method as described by Magalhaes et al. (2010). A volume of 50 μL of the lyophilized extracts of AC-p, MD-p, and SP-p, appropriately diluted, or standard gallic acid was combined with 50 μL of the Folin-Ciocalteu reagent (1:5 v/v) and allowed to rest for 2 min. Subsequently, 100 μL of NaOH (0.35 mol/L) was added, and the absorbance was measured at 760 nm using a Synergy HT1 microplate reader (Agilent, USA). The TPC was expressed in mg of gallic acid equivalent (GAE)/g, calculated from the standard gallic acid solution curve (0-0.5 mg/mL, R^2 = 0.999).

2.6.1.2. Fast Blue B assay. The TPC was quantified utilizing the Fast Blue B Salt method as described by Medina (2011). A volume of 100 μL of either standard gallic acid or appropriately diluted samples (lyophilized extracts of AC-p, MD-p, and SP-p) was combined with 50 μL of Fast Blue B Salt reagent (30 mg/100 mL) and 50 μL of NaOH (8.35 g/100 mL). The resulting mixture was allowed to rest for 10 min, followed by agitation for 3 s, after which the absorbance at 420 nm was measured using a Synergy HT1 microplate reader (Agilent, USA). The TPC was expressed in mg GAE/g, calculated from the standard curve (0-0.25 mg/mL, R^2 = 0.994). All analytical determinations were conducted in triplicate.

2.6.2. Identification of phenolic compounds using UHPLC-PDA-ESI-MS

The extraction of phenolic compounds was conducted following the methodology outlined by Tian, Laaksonen, Haikonen, Vanag, Ejaz, Linderborg, et al. (2019) with certain modifications. Anthocyanins were extracted using acidified methanol (methanol: hydrochloric acid, 99:1, *v/v*). Approximately 0.1–0.2 g of fruit peels were combined with 2 mL of acidified methanol, subjected to ultrasonication for 10 min (at room temperature, 45 kHz), and then centrifuged for 10 min (at 3200×*g*, 20 °C). The supernatants were collected post-centrifugation, and the precipitates underwent three additional extractions using the same procedure. The supernatants from all four extractions were pooled and concentrated to 1 mL under a nitrogen stream. For the extraction of non-anthocyanin phenolic compounds, fruit peels (0.8–0.9 g) were initially mixed with 5 mL of Milli-Q water and extracted with 10 mL of ethyl acetate for four times. This extraction was facilitated by ultrasonication (for 15 min, at room temperature, 45 kHz) and centrifugation (for 15 min, at 3200×*g*, 20 °C). The supernatants obtained after each extraction were evaporated to dryness at 30 °C using a vacuum rotary evaporator. The resulting residue was re-dissolved in 1 mL of methanol. Extracts of both anthocyanins and other phenolics were filtered through 0.22-μm PTFE filters and stored at −20 °C until subsequent LC-MS analysis.

Phenolic compounds in lyophilized extracts of AC-p, MD-p, and SP-p were analyzed using a Shimadzu ultra-performance liquid chromatography tandem mass spectrometry system (UHPLC-MS; Shimadzu Corp., Kyoto, Japan). This system was equipped with a liquid chromatograph triple-quadrupole mass spectrometer (LCMS-8045), an electrospray ionization interface (ESI), and an SPD-M40 photodiode array detector (PDA).

The LC separation was performed based on the method detailed in

the studies by Tian et al. (2019) with some modifications. In summary, 10 μL of the extract was injected into a Phenomenex Aeris peptide XB-C18 column (150 × 4.60 mm, 3.6 μm, Torrance, CA, USA) maintained at 25 °C, with a total flow rate of 1 mL/min. The mobile phases employed for anthocyanin analysis comprised 5.0% formic acid in Milli-Q water (5:95, formic acid: water, *v/v*, A) and acetonitrile (B). The LC gradient used in anthocyanin analysis was 0–1 min with 4–6% solvent B, 1–2 min with 6–8%B, 2–6 min with 8–9% B, 6–10 min with 9–10% B, 10–14 min with 10–11% B, 14–20 min with 11–12% B, 20–25 min with 12–24%B, 25–28 min with 24–80% B, 28–31 min with 80–4% B, and 31–35 min with 4% B. To analyze non-anthocyanin compounds, 0.1% formic acid in Milli-Q water (0.1:99.9, formic acid: water, *v/v*, A) and 0.1% formic acid in acetonitrile (0.1:99.9, formic acid: acetonitrile, *v/v*, B) were used as the mobile phases. The LC gradient was set as follows: 0-15 min with 5-10% solvent B, 15-20 min with 10-13% B, 20-25 min with 13-16% B, 25-30 min with 16-18% B, 30-35 min with 18-20% B, 35-40 min with 20-22% B, 40-45 min with 22-25% B, 45-50 min with 25-60% B, 50-55 min with 60-5% B, and 55-60 min with 4% B.

For MS analysis, MS was operated with 2 L/min of nebulizing gas flow, 15 L/min of heating gas flow, and 5 L/min drying gas flow. The temperatures of interface, desolvation, DL, and heat block were set as 300, 526, 150, and 400 °C, respectively. The eluents were flown into the MS system at a flow rate of approximately 0.3 mL/min. Full-scan MS and MS^2 product ion scans were performed in both positive and negative ionization modes. The mass range scanned was 120–1500 *m/z* for MS and 50–1500 *m/z* for MS^2. The MS^2 spectra were obtained by collision induced dissociation with collision energies (20 V under positive mode and 23 V under negative mode). The collision energies were optimized using external standards of caffeic acid, *p*-coumaric acid, ferulic acid, sinapic acid, 3-*O*-caffeoylquinic acid, quercetin 3-*O*-rutinoside, and quercetin 3-*O*-glucoside. The reference standards of anthocyanins (cyanidin 3-*O*-galactoside, cyanidin 3-*O*-glucoside, cyanidin, and peonidin), flavonols (myricetin 3-*O*-galactoside, myricetin 3-*O*-glucoside, myricetin, kaempferol 3-*O*-glucoside, quercetin 3-*O*-galactoside, quercetin 3-*O*-glucoside, quercetin, and isorhamnetin 3-*O*-rutinoside), flavan-3-ols ((+)-catechin and (−)-epicatechin), proanthocyanidins (procyanidin B2), and phenolic acids (ellagic acid, caffeic acid, 3-*O*-caffeoylquinic acid, 4-*O*-caffeoylquinic acid, and 5-*O*-caffeoylquinic acid) were also analyzed with the same method as that used in the analysis of peel extracts. The identification was based on comparison of MS/MS fragmentation patterns with both authentic commercial standards and literature-reported fragmentation data. MS data acquisition and processing, including peak detection and MS/MS interpretation, were performed using LabSolutions LCMS software (version 5.118, Shimadzu, Kyoto, Japan).

2.6.3. Antioxidant capacity

2.6.3.1. DPPH assay. The antioxidant capacities of lyophilized extracts of AC-p, MD-p, and SP-p were assessed utilizing a rapid high-throughput DPPH assay, as described by Cortés-Avendaño et al. (2024). In this procedure, 10 μL of either standard Trolox or appropriately diluted sample solutions were combined with 200 μL of DPPH working solution in a 96-well microplate. The working solution was prepared using a Tris-base buffer (10 mmol/L, pH 7.5) and methanol in a 1:1 vol ratio. Following a 10-min incubation period at room temperature, absorbance was measured at 520 nm using a Synergy HT1 multimodal microplate reader (Agilent, USA). The antioxidant capacity was quantified as μmol Trolox equivalent (TE)/g, derived from the standard curve (0-400 μM, $R^2 = 0.999$).

2.6.3.2. ABTS assay. The antioxidant capacities of lyophilized extracts of AC-p, MD-p, and SP-p were evaluated in triplicate utilizing the ABTS assay, as described by Cortés-Avendaño et al. (2024). The antioxidant capacities of AC-p-Lyo, MD-p-Lyo, and SP-p-Lyo were evaluated in triplicate utilizing the ABTS assay, as described by Cortés-Avendaño et al. (2024). A stock solution of $ABTS^+$ radicals was prepared by allowing the reaction between $ABTS^+$ (7 mmol/L) and potassium persulfate (2.45 mmol/L) to proceed for 16 h at room temperature in the absence of light. For the assay, 10 μL of Trolox, serving as an antioxidant standard, or an appropriately diluted sample (10 μL) was combined with 200 μL of the $ABTS^+$ radical working solution in a 96-well microplate. The mixture was incubated for 30 min at room temperature, and absorbance was measured at 734 nm using a Synergy HT1 microplate reader (Agilent, USA). The antioxidant capacity of the samples was expressed as μmol TE/g and was determined from the standard curve (0-400 μM, $R^2 = 0.998$).

2.6.3.3. ORAC assay. The evaluation of the oxygen radical absorbance capacity using fluorescein (ORAC-FL) for the samples, lyophilized extracts of AC-p, MD-p, and SP-p, was conducted following the methodology described by Ou et al. (2019), with specific modifications. The ORAC procedure entailed the combination of 25 μL of either blank, standard Trolox, or sample with 150 μL of fluorescein (FL) (137.22 nmol/L), followed by incubation for 30 min at 37 °C. Subsequently, 25 μL of AAPH (153 mmol/L) was introduced into a 96-well black microplate (Costar, Spain). All solutions were diluted in a phosphate buffer (7.5 mM, pH 7.4). The FL and AAPH were dispensed using an automatic injector, and all mixtures were prepared in the inner wells to minimize temperature variation effects. Distilled water was added to the remaining wells, and fluorescence measurements were taken every 2 min for 90 min at 37 °C after automatic shaking, with an excitation wavelength of 485 ± 20 nm and an emission wavelength of 528 ± 20 nm, using a Synergy H1 multimodal microplate reader (Agilent, USA). The ORAC values were calculated by determining the area under the curve (AUC) from the fluorescence ratio readings at various reaction times using GraphPad Prism software (GraphPad Software, CA, USA). These values were obtained in triplicate for each sample and expressed as μmol TE/g using a Trolox standard curve (0-100 μM, $R^2 = 0.990$).

2.6.3.4. Photochemiluminescence assay. The antioxidant capacity of lyophilized extracts of AC-p, MD-p, and SP-p against superoxide anion radicals generated from luminol upon exposure to UV light were measured using a Photochem® instrument (Analytik Jena, Leipzig, Germany) and analytical ACL and ACW kits (Popov & Lewin, 2005). The light emission curve was measured at 350 nm for 180 s and the inhibition of superoxide anion radicals was used to evaluate the antioxidant capacity of the samples. Data acquisition and analysis were performed using PCLsoft® control and analysis software (Analytik Jena, Leipzig, Germany). The antioxidant capacity was determined by triplicate using the area under the curve and was expressed as μmol TE/g from Trolox standard curve (0.5-3.0 nmol/L, $R^2 = 0.996$) for ACL and μmol GAE/g from gallic acid standard curve (0.5-4 nmol/L, $R^2 = 0.992$) for ACW.

3. Results and discussion

3.1. Characterization of Andean and tropical fruit peels

3.1.1. Particle size and distribution

The particle size of AC-p, MD-p, and SP-p were quantified using equivalent circular area diameter (ECAD). The median ECAD values for AC-p, MD-p, and SP-p were determined to be 60.8, 46.3, and 38.3, respectively, indicating a non-normal distribution across all samples (Fig. 3A, C and 3E). The kurtosis of ECAD is observed to be less than 3, indicating a platykurtic distribution characterized by thinner tails and fewer outliers, which suggests enhanced stability and a reduced likelihood of extreme values (Fig. 3). Skewness was assessed to quantify the asymmetry of the probability distribution relative to its mean. The variables MD-p and SP-p exhibited positive skewness in ECAD, signifying the presence of smaller particle sizes (Fig. 3C and E). Conversely,

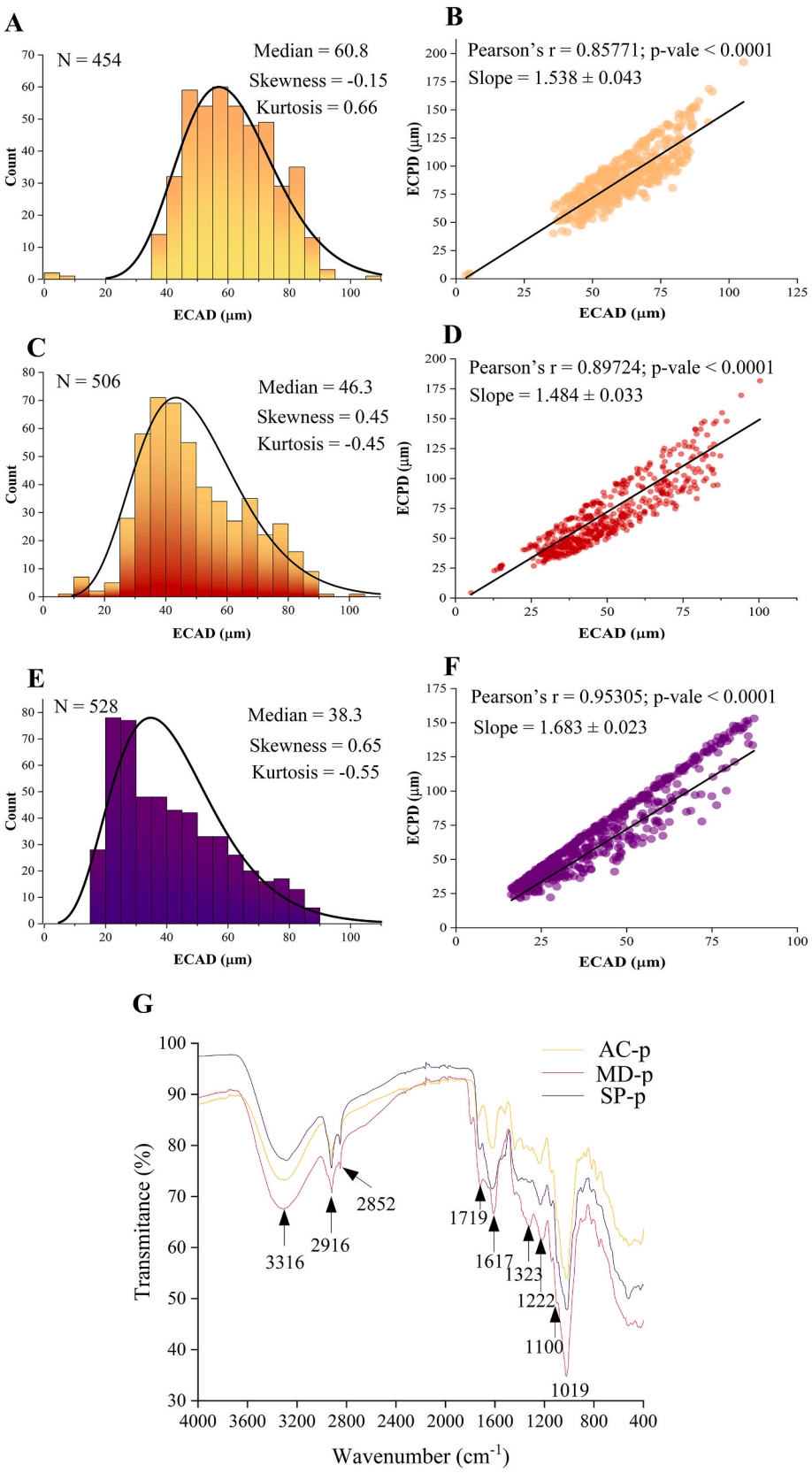

Fig. 3. Particle size and distribution and correlation analysis of peels of starfruit (AC-p) (A-B), camu camu (MD-p) (C-D), and elderberry (SP-p) (E-F). ECAD and ECPD are the equivalent circular area diameter and equivalent circular perimeter diameter, respectively. FT-IR spectra of AC-p, MD-p and SP-p (G), the values are mean of three replicates.

negative skewness in ECAD was identified for AC-p, indicating that the majority of particle sizes were concentrated on the right side of the distribution plot (Fig. 3A). The EPCD-ECAD dispersions illustrated the heterogeneity in particle size among the samples, with SP-p > MD-p > AC-p (Fig. 3B, D, and 3F).

Particle size and distribution are pivotal in determining the efficiency of UAE of phenolic compounds. A reduction in particle size enhances the surface area available to the solvent, thereby shortening diffusion pathways and expediting the mass transfer of phenolic compounds (Kobus et al., 2023). In the UAE of punicalagin, a hydrolysable tannic polyphenol, from pomegranate peel, a smaller particle size (<56 μm) yielded a 2.06-fold increase in the extraction of phenolic compounds compared to larger particle sizes (56-101 μm) (Cano-Lamadrid et al., 2023). Consistent with the findings of Papoutsis et al. (2018), the use of UAE on AC-p, MD-p, and SP-p can lead to further reduction in particle size, thereby enhancing solvent accessibility to the internal structures of plant materials and facilitating the extraction of phenolic compounds. Nevertheless, the reduction in particle size achieved through milling and ultrasound may be influenced by the insoluble fiber composition of the by-product peel of orange fruit (Liu et al., 2016). Although similar milling conditions (25000 rpm for 4 s) were applied to AC-p, MD-p, and SP-p, variations in particle size and distribution were observed among the samples, with AC-p > MD-p > SP-p. This discrepancy may be attributed to the differing insoluble fiber content in the peel of each by-product. The insoluble fiber content has been previously documented for AC-p (50.8 – 56.7 g/100 d.b.) (Chau et al., 2005) and MD-p (8.1 g/100 d.b.) (Cruz et al., 2024; Sidor & Gramza-Michałowska, 2015). However, the insoluble fiber content of SP-p remains unreported. Notably, the highest insoluble fiber content among the evaluated by-product peels was directly associated with their particle size. Ultrafine milling can reduce particle size to below 25 μm by disrupting hemicellulose, cellulose, and lignin (Hu et al., 2022; Qin, Dong, Tang, Chen, Xie, Cheng, et al., 2023). This process may enhance the homogeneity of particle size; however, smaller particles can diminish the efficiency of UAE. While very small particles facilitate high extraction yields, intermediate particle sizes may offer an optimal balance between extraction efficiency and energy consumption, as observed in matrices such as hemp and citrus residues (Kobus et al., 2023; Papoutsis et al., 2018).

3.1.2. FT-IR spectra

The FT-IR spectra of peel by-products (AC-p, MD-p, and NP-p) exhibited characteristic bands indicative of phenolic compounds and polysaccharides (Fig. 3G). A prominent band was observed at 3316 cm^{-1}, corresponding to the O-H stretching band of hydroxylic compounds, such as phenols, carboxylic acids, or alcohols (Almeida, Dias, Arriola, de Freitas, de Francisco, Petkowicz, et al., 2020; İşman et al., 2025). The peak at 2916 cm^{-1} was attributed to the C-H stretching vibration of alkyl and alkoxy groups (İşman et al., 2025). Additionally, the band at 2852 cm^{-1} indicated the stretching and bending vibrations of aliphatic alkane groups, including CH, CH_2, and CH_3 (Almeida et al., 2020). The peak at 1719 cm^{-1} was associated with the stretching vibration of the C-O bond of carbonyl groups, which are prevalent in pectin and hemicellulose (Almeida et al., 2020; Huo et al., 2023; İşman et al., 2025), which was predominant in the MD-p sample (Fig. 3G). The peak at 1617 cm^{-1} could be attributed to the esterified (1620 cm^{-1}) carboxyl groups in pectin (Huo et al., 2023) and/or to unsaturated compounds and the vibration of aromatic rings (İşman et al., 2025). The peaks at 1323, 1222, 1100, and 1019 cm^{-1} are related to the presence of cellulose and other polysaccharides (Fig. 3G). Specifically, the peak at 1327 cm^{-1} is associated with cellulose (1327 cm^{-1}) and esters and ethers (1227 cm^{-1}). Furthermore, the peaks at 1177 cm^{-1} and 1048 cm^{-1} were attributed to the pyranose ring in polysaccharides (İşman et al., 2025).

3.2. UAE of phenolic compounds from fruit peels at a small-scale laboratory

3.2.1. UAE parameters

The optimization of UAE for phenolic compounds was accomplished through the application of response surface methodology. This process incorporated independent variables such as sonication time, ultrasound power and amplitude, solvent-to-solid ratio, and the particle size of by-products (Fig. 1). However, the percentage amplitude and nominal ultrasound power deemed optimal under laboratory conditions are not scalable and do not facilitate the actual revalorization of by-products. In this study, the specific energy calibrated prior to each extraction process and the nominal amplitude were employed to ascertain the optimal UAE conditions.

The TPC was not influenced by the nominal amplitude of UAE (49 μm *vs* 63 μm) across all fruit peel by-products, specifically AC-p, MD-p, and SP-p, within the AED range of 25-125 J/mL (Fig. 4A–C). The ultrasonic amplitude is a critical factor in regulating cavitation intensity and mechanical shear, which in turn increases microstreaming and turbulence that influences mass transfer and cell disruption. An increase in amplitude typically enhances the phenolic yield up to an optimal level specific to the material in question (Sharayei et al., 2019). For instance, in the case of orange peels, an optimal sonicator relative amplitude of approximately 80% was found to maximize total polyphenols in aqueous ultrasonic-assisted extraction (UAE). Conversely, when employing a sonotrode on orange by-products, peak recovery was observed at very high amplitudes, around 90%, under extended sonication durations (Aguilar-Hernández, García-Magaña, Vivar-Vera, Sáyago-Ayerdi, Sánchez-Burgos, Morales-Castro et al., 2019; Foujdar et al., 2020). In this study, the extraction of TPC from AC-p, MD-p, and SP-p was achieved at a low AED. This indicates that the phenolic compounds are readily accessible to the solvent, obviating the need for high nominal amplitude ultrasound. On the other hand, respect to the influence of AED of UAE on TPC, for AC-p it was not showed differences at levels of 25, 50 and 125 J/mL, a decreasing or increasing were found at 75 and 100 J/mL respect that obtained at 25 J/mL, respectively (Fig. 4A). Ultrasound amplitude is a critical determinant of the acoustic intensity applied to a sample, significantly affecting the pressure, cavitation intensity, mass transfer, and cell disruption that facilitate phenolic release (Esteban-Lustres et al., 2022; Exposito-Almellon et al., 2025). In the current study, however, an increase in the nominal amplitude from 49 μm to 63 μm for AC-p did not correspond to the highest TPC extraction (Fig. 4A). This observation may be attributed to the characteristics of skin fruit by-products, which might necessitate lower amplitudes to effectively extract and preserve compounds. Consequently, although a higher TPC is extracted at the tested higher amplitude range (30-100%), the outcome is influenced by the food matrix and the specific compounds targeted for extraction (Aguilar-Hernandez, Garcia-Magana, Vivar-Vera, Sayago-Ayerdi, Sanchez-Burgos, Morales-Castro et al., 2019; Egues et al., 2021; Piasecka et al., 2022). Nonetheless, the optimal percentage amplitude in laboratory settings does not directly translate to pilot or industrial acoustic intensity (Exposito-Almellon et al., 2025). For MD-p, the maximum TPC extraction via UAE was observed at 25 J/m (Fig. 4B). For MD-p, the maximum TPC extraction via UAE was observed at 25 J/mL (Fig. 4B). This outcome may be attributed to the enhanced accessibility of the solvent to the peel fruit by-products, facilitated by sonication (Aguilar-Hernandez et al., 2019; Egues et al., 2021; Piasecka et al., 2022). Although similar TPC extraction levels were recorded at 50, 75, 100, and 125 J/mL for MD-p, a reduction in TPC was noted at these higher specific energies compared to 25 J/mL (Fig. 4B). This observation may indicate some degradation of anthocyanins in MD-p, as a decrease in monomeric anthocyanins has been documented for bilberry by-products under high ultrasonic intensity (Egues et al., 2021). For SP-p, a higher TPC was observed at 50 J/mL, comparable to that at 75, 100, and 125 J/mL, and greater than at 25 J/mL (Fig. 4C). Additionally, the TPC obtained was lower than that of AC-p and MD-p, which

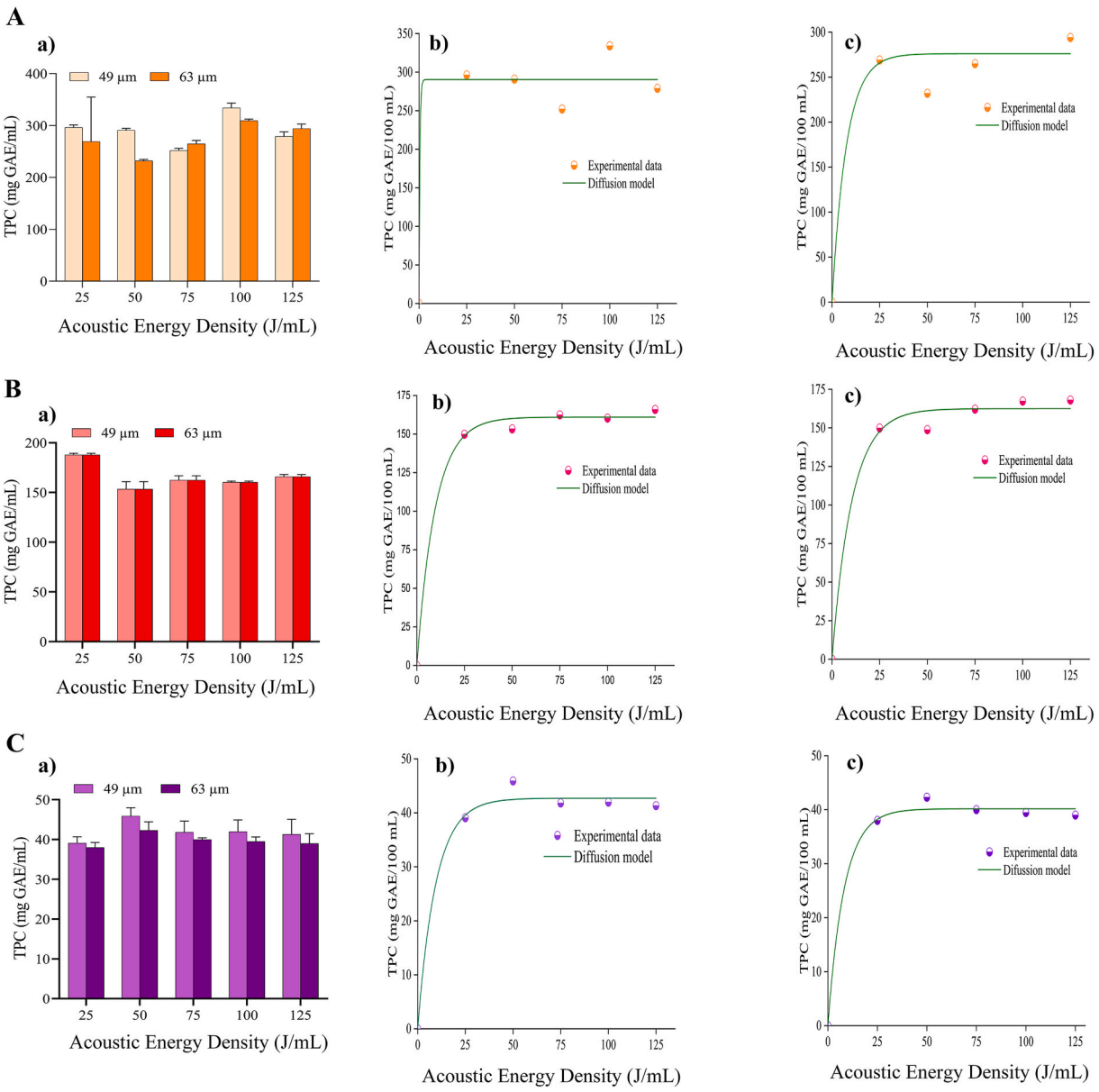

Fig. 4. Effect of nominal amplitude (μm) and acoustic energy density (AED) on ultrasound-assisted extraction (UAE) of phenolic compounds from starfruit (AC-p) (A-a), camu camu (MD-p) (B-b), and elderberry (SP-p) (C-c). UAE modelling of phenolic compound at nominal amplitude of 49 μm and 63 μm from AC-p (A-b and c), MD-p (B-b and c), and SP-p (C-b and c). The values are mean of three replicates.

may be partially attributed to the smaller particle size of SP-p (Fig. 3A, B and 3C), limiting solvent access for extracting phenolic compounds from the matrix. Particle size is recognized as a significant variable influencing the recovery of specific phenolics in citrus pomace, pomegranate, tropical peels, nutshells, and carobs, suggesting that physical access to intracellular compounds mediates the performance of UAE. The optimal particle size is contingent upon the structure of the fruit by-product, the target phenolic class, and the processing context. For various fruit matrix by-products, optimal sizes range from sub-100 μm to the millimeter scale, reflecting differences in tissue hardness, compound localization, and the risk of powder agglomeration or inadequate solvent flow at extremes (Cano-Lamadrid et al., 2023; Papoutsis et al., 2018).

The UAE has been widely utilized as a non-thermal and environmentally sustainable method for extracting various compounds from agro-industrial by-products, thereby contributing to their valorization within the framework of sustainable development through the recovery of functional compounds (Ahmad et al., 2024; Areti, Muleta, Abo, Hamda, Adugna, Edae, et al., 2024; Boateng & Clark, 2024). However, few studies have focused on the peels of the tropical fruits applied in our research. Cuna (2018) suggested that employing UAE at 135 W power and 50 °C for 1, 6, 12, and 24 h can extract phenolic acids and flavonoids from both green and red peels of camu camu. Reports on the use of UAE extraction of phenolic compounds from the peels of star fruit and elderberry are relatively rare.

3.2.2. *Mathematical modelling*

The experimental data related to TPC were examined utilizing a diffusion model, with AED serving as an independent variable. AED is defined as the energy dissipated per unit volume of the treated samples. As an intensive parameter, AED remains constant irrespective of the equipment scale, thereby providing valuable insights for scale-up considerations (Chan et al., 2017; Natolino & Celotti, 2022). TPC was well adjusted to the diffusion model for all peel fruit by-products AC-p, MD-p and SP-p with coefficient of determination R^2-adjusted of 0.934-0.940, 0.988-0.996 and 0.987-0.994, respectively. The apparent first-order rate constant (k) ranged from 0.096 to 2.29 mg GAE/J and maximum

TPC from 40.2 to 290.5 mg GAE/mL. The effect of amplitude on TPC did not show statistical differences and only AED 25 J/mL is necessary to extract the maximum TPC for all studied peel fruit by-products (Fig. 4A-B-b and C-b and 4A-c, B-c and C-c). Therefore, for the laboratory scale up for the phenolic compound extraction a EAD of 25 J/mL and amplitude 49 μm were chosen.

3.2.3. UAE process monitoring

The net power (W) and temperature (°C) during the sonication at 24 kHz of each fruit peel by-product (AC-p, MD-p, and SP-p) in the UAE exhibited distinct profiles for each AED level (Fig. 5 and Supplementary material 2). The ultrasonic net power followed a decreasing order of AC-p > MD-p > SP-p for AED of 50, 75, 100, and 125 J/mL at amplitudes of 49 μm and 63 μm (Fig. 5 and Supplementary material 2). This trend corresponded with the particle size and distribution of the ground AC-p (median = 60.8 μ; skewness = −0.15; kurtosis = 0.66), MD-p (median = 46.3 μ; skewness = 0.44; kurtosis = −0.45), and SP-p (median = 38.3 μ; skewness = −0.15; kurtosis = 0.66) (Fig. 3). The net energy of ultrasound, whether input or local AED, is correlated with changes in particle size through mechanisms such as acoustic propulsion, fragmentation, ablation, and wet milling. Generally, an increase in local AED enhances the acoustic forces exerted on particles, thereby promoting a reduction in their size (Brysev et al., 2019; Voβ & Wittkowski, 2023). For nano- and micro-particles, the propulsion velocity exhibited an approximately linear increase with both particle size and AED, suggesting that larger particles experience stronger net acoustic forces at a given energy density (Voβ & Wittkowski, 2023). This phenomenon was observed for AC-p, MD-p, and SP-p in the current study. Furthermore, the maximum temperature was attained for fruit peel by-products AC-p and MD-p in comparison to SP-p (Fig. 5 and Supplementary material 2), which is directly associated with the highest ultrasound net power that enhances viscosity heat dissipation (Hielscher, 2012). In contrast, at 25 J/mL, the inverse relationship between ultrasound net power and the particle size of AC-p, MD-p, and SP-p was not feasible, as the AED was insufficient to facilitate the acoustic propulsion of the particles (Fig. 5 and Supplementary material 2). The association between temperature increase and particle size at varying sonication durations in ROI = R1 was substantiated through kinetic thermal analysis. In the absence of particles, the temperature rise in ethanol aqueous solution (30% v/v) was less pronounced compared to samples containing the peel fruit by-products AC-p, MD-p, and SN-p (Fig. 6A). The Thermal Spatial Complexity Index (TSCI) was utilized to characterize the spatial variation in the temperature of the region of interest (ROI) during sonication, with analyses conducted at 1-s intervals (Fig. 6B). TSCI incorporates the mean, variance, and Shannon entropy, thereby enabling the determination of the spatial complexity of thermal profiles during sonication. The ethanol aqueous solution 30% *v/v* and SN-p samples exhibited lower TSCI values compared to the MD-p and AC-p samples (Fig. 6B). This discrepancy can be attributed to the presence or absence of solids or variations in solid particle size (Fig. 3A, C, and 3E). These differences in temperature homogeneity during sonication have been linked to internal structural barriers arising from interactions with solid samples (Santos et al., 2021) and the structural properties of the solids, such as the presence of crystalline structures (Rojas-Lima et al., 2021). The increase in y_{max} and the decrease in the HillSlope of the sigmoidal dose-response curve also reflected the increasing order of TSCI: AC-p > MD-p > SP-p > ethanol aqueous solution 30% v/v. The HillSlope values were 0.098, 0.074, 0.215, and 0.131 for AC-p, MD-p, SP-p, and ethanol aqueous solution (30% v/v), respectively (Fig. 6C).

3.2.4. UAE laboratory scale-up

Prior to comparing the TPC obtained from AC-p, MD-p, and SP-p through ultrasound extraction using two distinct probes, Sys-S24d7 (7 mm) and Sys-24d14 (14 mm), the effects of probe and vessel diameters, liquid sample height, and immersion depth were examined. The diameters of the probe and vessel are influenced by power density, cavitation volume, and cavitation fraction, which in turn affect the extraction rate, yield, and energy efficiency (Bampouli et al., 2024; Nanzai et al., 2009; Yi et al., 2012). Smaller reactors enhance acoustic power density, whereas larger reactors offer a greater cavitation volume, thereby increasing the absolute yield (Krzywicka & Kobus, 2023; Nanzai et al., 2009; Yi et al., 2012). Additionally, the immersion depth can enhance process efficiency by extending cavitation zones into the bulk (Ebrahimi et al., 2018). These geometric parameters were modified for the extraction of phenolic compounds using the ultrasound probes Sys-S24d7 and Sys-24d14. Factors related to the ratio of probe diameter to vessel diameter and the immersion depth ratio for each probe were employed to adjust the experimental TPC data. The TPC extracted with Sys-S24d7 and Sys-24d14 was comparable across all peel fruit by-products, namely AC-p, MD-p, and SP-p (Fig. 7A).

3.3. Characterization of peel extracts obtained from laboratory scale-up UAE

3.3.1. Total and profiles phenolics

The TPC of AC-p, MD-p, and SP-p, as determined by the (FB) assay, was observed to be higher than that obtained using the (FC) assay, following the order: SP-p > AC-p > MD-p (Fig. 7B). This observation aligns with previous research indicating that the FB method consistently produces higher gallic TPC values than the FC method across various samples, including juices, fresh fruits, and dried fruits (Medina, 2011). A plausible explanation for this discrepancy is that the FC assay indirectly measures phenolics and is prone to interference from various non-phenolic reducing substances. In contrast, the FB assay provides a more direct and specific quantification of phenolic compounds, resulting in higher values by avoiding such interferences (Medina, 2011).

The extracts of AC-p, MD-p, and SP-p, obtained under optimal ultrasound conditions, encompassed a diverse array of phenolic compounds (Table 1). A total of 50 compounds were identified, categorized into flavonols (17 compounds), proanthocyanidins (13), hydroxycinnamic acids (10), anthocyanins (6), flavan-3-ols (2), flavones (1), and hydroxybenzoic acids (1). The identification process was conducted through the comparison of UV absorption and MS fragmentation with reference standards or data from previous studies (Biswal et al., 2022; da Silva, Scapim, da Silva, Stafussa, Aranha, Jorge, et al., 2023; Duymus et al., 2014; Fracassetti, Costa, L., & Tomás-Barberán, 2013; Islam et al., 2020; Kiselova-Kaneva et al., 2022; Lin et al., 2014; Rush et al., 2018; Tian, Liimatainen, Alanne, Lindstedt, Liu, Sinkkonen, et al., 2017; Uzlasir et al., 2020).

The AC-p extract was found to contain seventeen phenolic compounds, comprising one flavanol, one flavone, two anthocyanins, two flavan-3-ols, and eleven proanthocyanidins (Fig. 7C–F and Table 1). Notably, a methyl derivative of cyanidin was identified. This compound was further verified not to be peonidin (3′-*O*-methyl-cyanidin) based on the distinct retention times observed in the LC chromatogram. In line with the findings of Biswal et al. (2022), the AC-p extract was found to contain catechin, epicatechin, procyanidin dimers, and glycosylated apigenin. Similarly, phenolic compounds such as epicatechin, catechin, and B-type procyanidins have been identified in the bark of *Averrhoa carambola* L. (Islam et al., 2020). The main phenolic components identified in the MD-p extract were anthocyanins (such as cyanidin and its glycosides) (Fig. 7F and Table 1), hydroxycinnamic acids (different isomers of caffeoylquinic acid), glycosylated flavonols (myricetins, kaempferols, and quercetins), epicatechin derivatives, and ellagic acid and its glycosylated form (Fig. 7D and Table 1). Chlorogenic acid (3-*O*-caffeoylquinic acid) has been detected in the MD-p, although at low concentrations. In contrast, it was the predominant phenolic compound in the MD-p extract studied, showing a high-intensity peak in the LC chromatogram. These differences may be due to the geographical origin and maturity of camu camu (da Silva et al., 2023). Ellagic acid was identified in the MD-p extract studied, as previously reported in camu camu peels (Cuna, 2018). Although quercetin derivatives have been

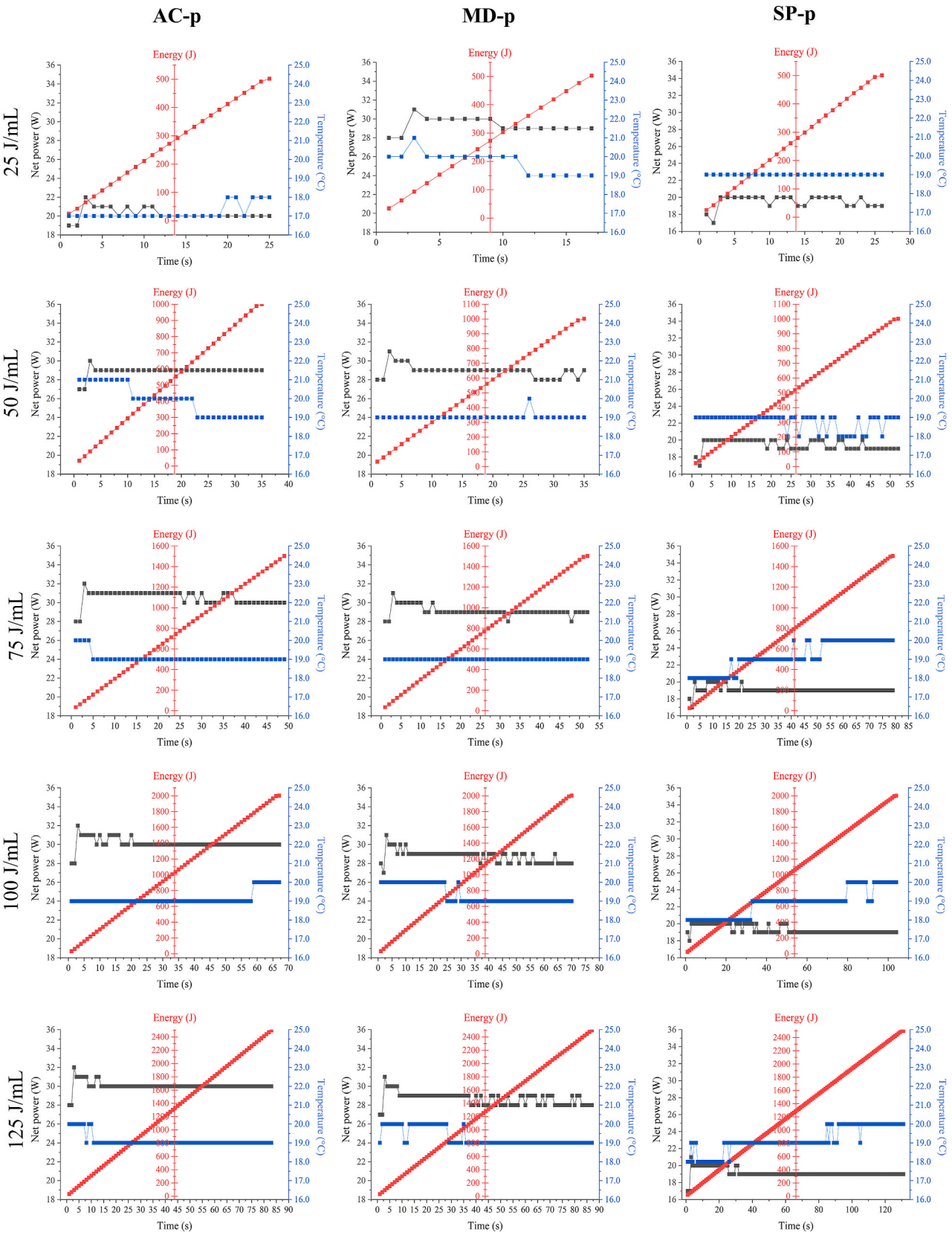

Fig. 5. Total energy, net power and temperature of ultrasound-assisted extraction of phenolic compounds from starfruit (AC-p), camu camu (MD-p), and elderberry (SP-p) at 25, 50, 75, 100 and 125 J/mL and nominal amplitude of 49 μm. The values are mean of three replicates.

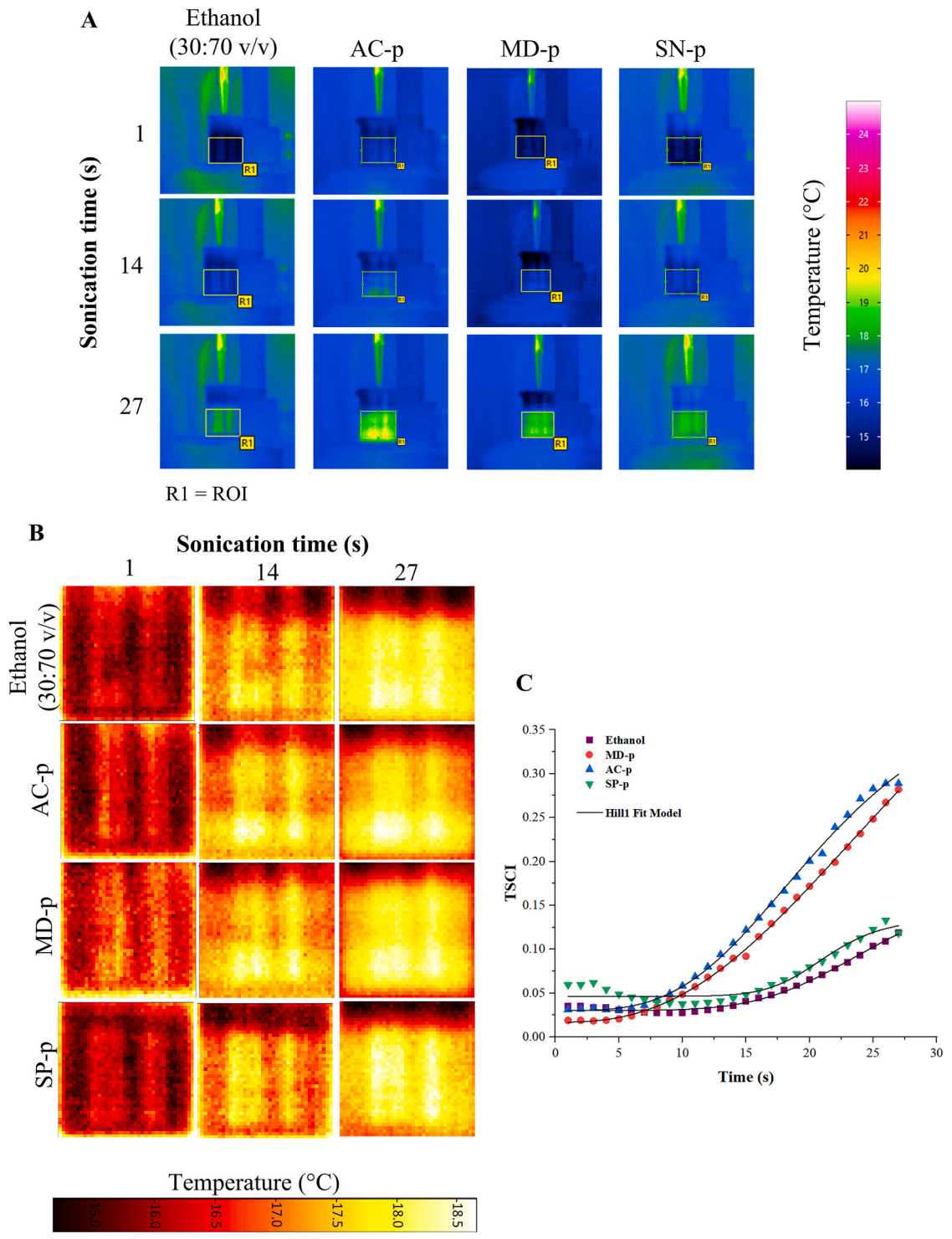

Fig. 6. Thermal images of ultrasound-assisted extraction of phenolic compounds from starfruit (AC-p), camu camu (MD-p), and elderberry (SP-p) at 25 J/mL and nominal amplitude of 49 μm. Thermal image of small-scale ultrasound system (A) and Region of Interest (ROI) (B) and Thermal Spatial Complexity Index (TSCI) within the ROI (C). Ethanol aqueous solution 30% v/v was used as control. The values are mean of three replicates.

identified in the peel, their concentrations have not yet been documented (Conceicao, Albuquerque, Pereira, Correa, Lopes, Calhelha, et al., 2019; Cuna, 2018). Consistent with the findings of Conceicao et al. (2019), cyanidin-3-*O*-glucoside was identified as the main pigment in the MD-p extract, accompanied by cyanidin-hexoside-pentoside (Fig. 7F and Table 1). The phenolic compounds detected in the SP-p extract mainly included cyanidins, quercetins, procyanidins, caffeoylquinic acids, and dicaffeoylquinic acids (Fig. 7E and Table 1). In a previous study, Porras-Mija et al. (2020) identified chlorogenic acid and catechin in the fruit of *Sambucus peruvian*. Furthermore, a isomer of cyanidin-hexoside-pentoside and cyanidin 3-*O*-glucoside were identified as main anthocyanins (Fig. 7F and Table 1) similar to those reported by Porras-Mija et al. (2020) and Pangestu et al. (2020).

3.3.2. *Antioxidant capacity*

Lyophilized extracts from AC-p, MD-p, and SP-p showed antioxidant

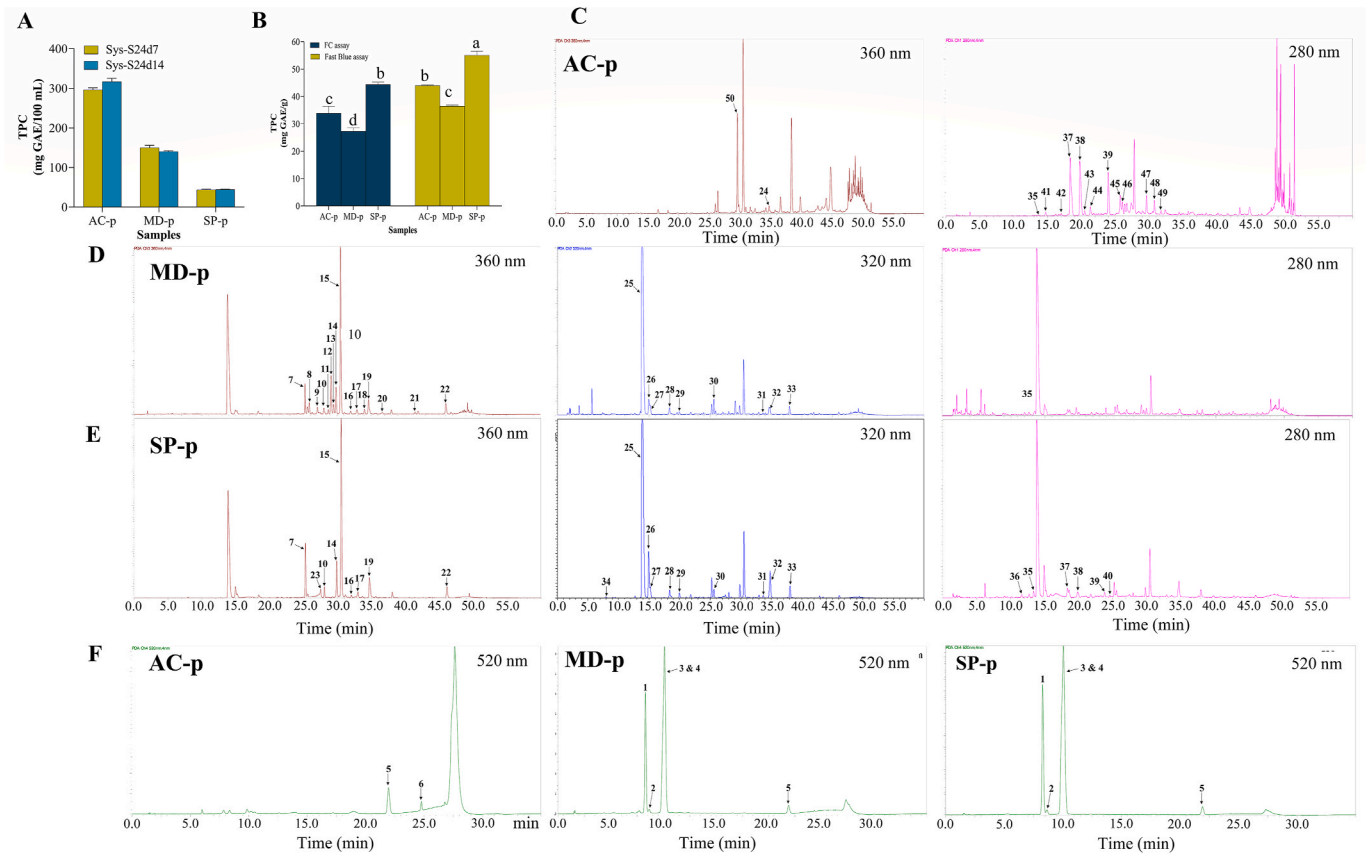

Fig. 7. Phenolic compounds from starfruit (AC-p), camu camu (MD-p), and elderberry (SP-p) extracted by small-scale (Sys-S24d7) and scale-up (Sys-S24d7) laboratory ultrasound systems at 25 J/mL and nominal amplitude of 49 μm (A). Total phenolic content (TPC) (B), phenolic compounds profile (C, D, E), anthocyanin profile (F) of extracts obtained by UAE from AC-p, MD-p and SP-p using the Sys-S24d7 system at 25 J/mL and nominal amplitude of 49 μm. The phenolic compounds and anthocyanins identified in the lyophilized extracts of AC-p, MD-p and SP-p are described in Table 1. The values are mean of three replicates.

activity in tests like DPPH, ABTS, ORAC, and photoluminescence (Fig. 8A–B). The AC-p sample had an antioxidant capacity of 223.1 ± 6.5 μmol TE/g against DPPH. This is less than the 1000 μmol TE/g for starfruit peel extract (Matsusaka & Kawabata, 2010) but more than the 15 μmol TE/g for whole starfruit (Ganoza-Yupanqui, Muñoz-Acevedo, Ybañez-Julca, Mantilla-Rodriguez, Zavala, Gajardo, et al., 2021). For ABTS, AC-p had 466.7 μmol TE/g, higher than starfruit pomace (204.7-228.26 μmol TE/g db) (Pantaleón-Velasco et al., 2014) and peel extracts (~36 μmol TE/g) (Ganoza-Yupanqui et al., 2021). The starfruit peel extract had the highest ABTS antioxidant capacity (~900 μmol TE/g) (Matsusaka & Kawabata, 2010). These differences may be due to factors like fruit type, growing conditions, ripeness, and fruit part. Thus, starfruit pulp has much less antioxidant capacity than the peel (Matsusaka & Kawabata, 2010). Moreover, AC-p showed also antioxidant capacity against peroxyl (ORAC values = 510.7 μmol TE/g) and superoxide anion (O_2^-) (PL-ACW = 413.2 ± 16.6 μmol GAE/g and PL-ACL = 2378.7 ± 172.1 μmol TE/g) (Fig. 8A–B). In our knowledge this is the first report for starfruit peel.

The MD-p sample demonstrated an antioxidant capacity of 138.1 ± 6.4 μmol TE/g against DPPH, which is lower than that of the ethanolic extract of whole fruit camu camu, recorded at 2571.34 ± 31.5 μmol TE/g (Pimenta da Silva et al., 2023). In contrast, the lyophilized MD-p extract exhibited a higher antioxidant capacity when evaluated using the ABTS assay, with a value of 154.2 ± 1.2 μmol TE/g, compared to the 135 μmol TE/g reported for the peel extracts assessed using the ABTS/ABAP assay (Ganoza-Yupanqui et al., 2021). However, the ORAC antioxidant capacity of the lyophilized MD-p extract (483.1 ± 0.2 μmol TE/g) was comparable to that of the ethanolic camu camu extract, which was 485.01 ± 55.85 μmol TE/g (Pimenta da Silva et al., 2023). Additionally, the MD-p sample exhibited antioxidant capacity measured by photoluminescence with PL-ACW and PL-ACL values of 4526.4 ± 95.1 μmol TE/g and 4964.6 ± 623.4 μmol GAE/g, respectively (Fig. 8B). The lyophilized SP-p extract obtained via ultrasound exhibited a DPPH antioxidant capacity of 307.6 ± 5.0 μmol TE/g, which is lower than the values reported for the aqueous extract of various *S. nigris* ranged from 620 to 710 μmol TE/g (Mandrone et al., 2014). Similarly, the antioxidant capacity of the SP-p sample, as measured by the ABTS assay (186.9 ± 5.1 μmol TE/g db), was lower than that observed in elderberry (*Sambucus nigra* subsp. *peruviana*) from four Peruvian regions (272-337 μmol TE/g db) (Porras-Mija et al., 2020). However, the DPPH and ABTS antioxidant capacities of the SP-p sample were higher than those reported for the aqueous extract of elderberry bagasse (*Sambucus peruviana* Kunth), which were 65 μmol TE/g dw and 66 μmol TE/g dw, respectively (Rojas-Ocampo et al., 2021). The ORAC antioxidant capacity of the lyophilized SP-p extract (882.9 ± 2.3 μmol TE/g) was comparable to those reported for elderberry (*Sambucus nigra* subsp. *peruviana*), which ranged from 677 to 1165 μmol TE/g dw (Porras-Mija et al., 2020). , which ranged from 677 to 1165 μmol TE/g dw (Porras-Mija et al., 2020). Furthermore, as anticipated, the SP-p sample also inhibited O_2^-, with PL-ACL = 2617.18 ± 17.4 μmol TE/g and PL-ACW = 622.44 ± 54.4 μmol GAE/g (Fig. 8B).

4. Conclusion

Phenolic compounds were extracted from the peels of starfruit (AC-p), camu camu (MD-p), and elderberry (SP-p) utilizing acoustic specific energy (AED) and nominal amplitude as laboratory scale-up parameters, facilitating the revalorization of food by-products within a genuine

Table 1
Phenolic profile measured by UHPLC-PDA-ESI-MS of starfruit (AC-p), camu camu (MD-p), and elderberry (SP-p) peel extracts.

No.	Identification	UV λ_{max} (nm)	MS (*m/z*)		MS^2 (*m/z*)	Distribution	Level of identification[a]
			$[M-H]^-$/ $[2M-H]^-$	$[M+H]^+$/ $[M+Na]^+$			
Anthocyanins							
1	Cyanidin-hexoside-pentoside 1	517	578.9/-	581.0/-	581.0 → **287.3**	MD-p, SP-p	Level 2, Literature [1]
2	Cyanidin 3-*O*-galactoside	516	447.0/-	449.0/-	449.0 → **287.1**	MD-p, SP-p	Level 1, Literature [1]
3	Cyanidin-hexoside-pentoside 2	514	579.0/-	581.0/-	581.0 → **287.3**	MD-p, SP-p	Level 2, Literature [1,2]
4	Cyanidin 3-*O*-glucoside	513	447.0/-	449.0/-	449.0 → **287.1**	MD-p, SP-p	Level 1, Literature [2–4]
5	Cyanidin	520	285.0/-	287.1		AC-p, MD-p, SP-p	Level 1, Literature [5]
6	methyl-Cyanidin	521	299.0/-	301.0/-	301.0 → **286.0**, 258.1	AC-p	Level 3
Flavonols							
7	Quercetin-hexoside-hexoside	254, 351	625.1/-	627.0/649.0	627.0 → **303.0** 625.1 → **300.0**	MD-p, SP-p	Level 2, Literature [6]
8	Myricetin 3-*O*-galactoside	258, 354	479.1/-	481.0/503.0	481.0 → **318.9** 479.1 → **315.9**	MD-p	Level 1, Literature [3]
9	Myricetin-pentoside 1	261, 351	449.1/-	451.0/473.0	451.0 → **319.1** 449.1 → **316.1**	MD-p	Level 2, Literature [3]
10	Kaempferol-hexoside-hexoside	262, 344	609.1/-	611.0/633.0	611.0 → **287.1** 609.1 → **285.1**	MD-p, SP-p	Level 2, Literature [6]
11	Myricetin-pentoside 2	262, 352	449.1/-	451.0/473.0	451.0 → **319.1** 449.1 → **316.1**	MD-p	Level 2, Literature [3]
12	Myricetin-pentoside 3	253, 350	449.1/-	451.0/473.0	449.1 → **316.1**	MD-p	Level 2, Literature [3]
14	Quercetin 3-*O*-galactoside	253, 351	463.0/-	465.0/487.0	465.0 → **303.0** 463.0 → **300.1**	MD-p, SP-p	Level 1, Literature [3,6,7]
15	Quercetin 3-*O*-glucoside	253, 351	463.0/-	465.0/487.0	465.0 → **303.0** 463.0 → **300.1**	MD-p, SP-p	Level 1, Literature [3,6,7]
16	Quercetin-pentoside 1	263, 345	433.0/-	435.0/457.0	435.0 → **303.0** 433.0 → **300.2**	MD-p, SP-p	Level 2, Literature [3,7]
17	Kaempferol-hexoside	262, 345	447.1/-	449.0/471.0	449.0 → **287.0**	MD-p, SP-p	Level 2, Literature [7]
18	Quercetin-pentoside 2	254, 346	433.1/-	435.0/457.0	435.0 → **303.0** 433.1 → **300.1**	MD-p	Level 2, Literature [3,7]
19	Kaempferol 3-*O*-glucoside	262, 343	447.1/-	449.0/471.0	449.0 → **287.0** 447.1 → **285.1**	MD-p, SP-p	Level 1, Literature [7]
20	Myricetin	265, 363	317.1/-	319.0/-		MD-p	Level 1, Literature [3,4]
21	Myricetin-coumaroylhexoside	265, 355	625.0/-	627.0/649.0	627.0 → **319.1** 625.0 → **316.1**	MD-p	Level 3
22	Quercetin	252, 367	301.1/-	303.0/-		MD-p, SP-p	Level 1, Literature [4]
23	Quercetin-deoxyhexoside-glucuronide	253, 350	623.1/-	625.0/647.0	625.0 → **303.0**	SP-p	Level 3
24	Isorhamnetin 3-*O*-rutinoside	266, 350	623.1/-	625.0/647.0	625.0 → **317.2** 623.1 → **314.7**	AC-p	Level 1, Literature [6]
Hydroxybenzoic acid derivatives							
13	Ellagic acid	250	301.1/-	303.0/-		MD-p	Level 1, Literature [3,4]
Hydroxycinnamic acid derivatives							
25	3-*O*-Caffeoylquinic acid	290(sh), 322	353.1/707.1	355.0/377.0	355.0 → **163.1** 353.1 → **191.1**	MD-p, SP-p	Level 1, Literature [4,6,7]
26	Caffeic acid	290(sh), 328	179.2/359.1	181.0/-		MD-p, SP-p	Level 1, Literature [1]
27	4-*O*-Caffeoylquinic acid	290(sh), 323	353.2/707.1	355.1/377.0	355.1 → **163.1** 353.2 → **191.1**	MD-p, SP-p	Level 1, Literature [4,6,7]
28	Caffeoylquinic acid 3	290(sh), 311	353.2/707.1	355.1/377.1	355.1 → 193.1, **163.0** 353.2 → **191.2**	MD-p, SP-p	Level 2, Literature [4,6,7]
29	Coumaroylquinic acid	290(sh), 306	337.2/-	339.1/361.0	339.1 → **147.1** 337.2 → **191.2**	MD-p, SP-p	Level 2, Literature [6,7]
30	Feruloylquinic acid	290(sh), 324	367.1/735.1	369.0/391.0	369.0 → 163.1, 145.1 367.1 → 179.2, 161.1	MD-p, SP-p	Level 2, Literature [6,7]
31	Dicaffeoylquinic acid 1	290(sh), 317	515.1/-	517.1/539.0	515.1 → **353.0**, 209.1, 173.1	MD-p, SP-p	Level 2, Literature [6]
32	Dicaffeoylquinic acid 2	290(sh), 324	515.1/-	517.0/539.0	515.1 → **353.4**, **191.1**	MD-p, SP-p	Level 2, Literature [6]
33	Dicaffeoylquinic acid 3	290(sh), 324	515.1/-	517.0/539.0	517.0 → **163.1** 515.1 → **353.4**, 203.3, **191,1**, 172.9	MD-p, SP-p	Level 2, Literature [6]
34	5-*O*-Caffeoylquinic acid	290(sh), 322	353.2/-	355.1/377.0	353.2 → **191.2**, 179.2	SP-p	Level 1, Literature [4,6,7]
Flavan-3-ols							
35	(+)-Catechin	280	289.1/579.1	291.1/-	291.1 → 207.1, 165.2, 161.1, 147.1, 139.0, 123.1, 119.1 289.1 → 245.0, 220.9, 202.9, 186.3, 162.4, 150.5, 137.4	AC-p, MD-p, SP-p	Level 1, Literature [5,7,8]

(*continued on next page*)

Table 1 (*continued*)

No.	Identification	UV λ_{max} (nm)	MS (*m/z*)		MS^2 (*m/z*)	Distribution	Level of identification[a]
			$[M-H]^-$/ $[2M-H]^-$	$[M+H]^+$/ $[M+Na]^+$			
38	(−)-Epicatechin	278	289.1/579.1	291.0/-	291.1 → 207.1, 179.1, 165.1, 161.2, 147.0, 139.0, 123.0, 119.1 289.1 → 244.8, 221.1, 203.2, 187.3, 160.1, 151.3, 137.3, 125.2, 123.4, 109.2	AC-p, SP-p	Level 1, Literature [5,7,8]
Proanthocyanidins							
36	B-type procyanidin dimer 1	276	577.1/-	579.0/-	579.0 → 475.3, 427.0, 409.1, **291.0**, 289.1 577.1 → **451.4**, **425.2**, **407.1**, **289.3**, **287.1**	SP-p	Level 2, Literature [7,9,10]
37	Procyanidin B2	285	577.1/-	579.0/-	579.0 → 427.1, 409.1, **291.1**, 289.1 577.1 → **425.1**, **407.3**	AC-p, SP-p	Level 1, Literature [5,7–10]
39	B-type procyanidin trimer 1	278	865.1/-	867.0/-	867.0 → 715.0, **579.0**, 425.1, 289.1 865.1 → **713.0**, **576.9**, 545.0, **451.3**, 405.0, **289.3**	AC-p, SP-p	Level 2, Literature [7,9,10]
40	B-type procyanidin dimer 2	278	577.1/-	579.0/-	579.0 → 432.7, 427.3, 408.9, **291.1** 577.1 → **451.1**, **425.3**, 409.0, **288.9**	SP-p	Level 2, Literature [7,9,10]
41	B-type procyanidin dimer 3	276	577.1/-	579.0/-	579.0 → 452.9, 427.2, 409.2, **291.1**, 289.1 577.1 → **451.1**, **425.1**, **407.2**, **289.0**	AC-p	Level 2, Literature [7,9,10]
42	B-type procyanidin dimer 4	278	577.1/-	579.0/-	579.0 → 427.2, 409.2, **291.2**, 289.0 577.1 → **451.1**, **424.9**, **407.1**, **289.1**	AC-p	Level 2, Literature [7,9,10]
43	B-type procyanidin tetramer 1	275	1153.1/-	1155.0/-		AC-p	Level 2, Literature [10]
44	B-type procyanidin tetramer 2	277	1153.1/-	1155.1/-		AC-p	Level 2, Literature [10]
45	B-type procyanidin tetramer 3	277	1153.1/-	1155.1/-		AC-p	Level 2, Literature [10]
46	B-type procyanidin trimer 2	276	865.1/-	867.0/-	865.1 → **713.1**, 695.0, **591.1**, **577.1**, **574.7**, **425.2**, **406.7**, **288.8**	AC-p	Level 2, Literature [7,9,10]
47	B-type procyanidin dimer 5	275	577.1/-	579.0/-	579.0 → 433.2, 427.0, 409.2, **291.1**, 289.3	AC-p	Level 2, Literature [7,9,10]
48	B-type procyanidin dimer 6	276	577.1/-	579.0/-	579.0 → 433.2, 427.0, 409.2, **291.1**, 289.3 577.1 → **451.3**, **425.1**, **407.0**, **289.1**, **287.2**	AC-p	Level 2, Literature [7,9,10]
49	B-type procyanidin trimer 3	276	865.1/-	867.0/-	867.0 → 714.9, **579.1**, **291.2**, 289.1 865.1 → **712.8**, 630.2, 463.2, **451.3**, **407.0**, **289.1**, **286.6**	AC-p	Level 2, Literature [7,9,10]
Flavones							
50	Apigenin-hexoside	268, 335	431.1/-	433.0/-	433.0 → **415.1**, **397.0**, **367.1**, 322.9, **312.8**, 283.0, **271.1**	AC-p	Level 2, Literature [5]

Reference literature includes: 1. Tian et al. 2017, 2. Duymus et al., 2014; 3. Fracassetti et al. 2013, 4. da Silva et al. 2023, 5. Biswal et al. 2022, 6. Uzlasir et al., 2020; 7. Kiselova-Kaneva et al. 2022, 8. Islam et al. 2020, 9. Rush et al. 2018, 10. Lin et al. 2014.

[a] Identification levels are assigned according to Metabolomics Standards Initiative (MSI) guidelines: Identified compounds confirmed with authentic standards (Level 1), identified compounds based on previous research (Level 2), and putatively characterized compounds (Level 3).

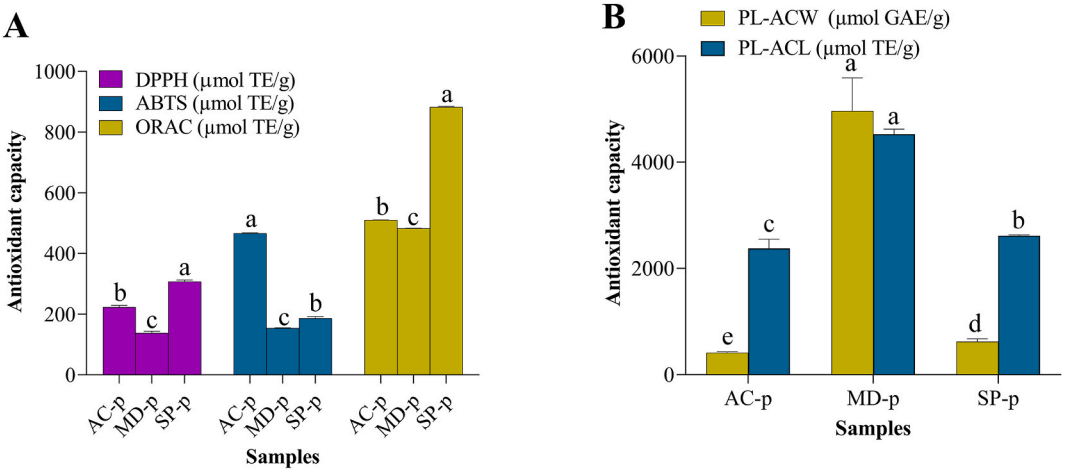

Fig. 8. Antioxidant capacity of extracts obtained by UAE from AC-p, MD-p and SP-p using the Sys-S24d7 system at 25 J/mL and nominal amplitude of 49 µm. The values are mean of three replicates. Distinct letters indicate statistically significant differences as determined by Tukey's test ($P < 0.05$).

circular economy framework. The characterization of tropical peel by-products, particularly their particle size distribution, demonstrated its impact on the ultrasound-assisted extraction of phenolic compounds, influencing extraction efficiency, kinetic modelling, and the necessity to establish specific milling conditions to ensure optimal ultrasound-assisted extraction. The phenolic compound content extracted via ultrasound from AC-p, MD-p, and SP-p, as well as AED, was modeled using a modified diffusion model derived from Fick's second law. Detailed monitoring of the ultrasound extractions revealed a direct correlation between ultrasonic heating and the particle size of the samples, which

was validated for the first time using the Thermal Spatial Complexity Index (TSCI) calculated from kinetic thermal analysis. The scale-up of ultrasound-assisted extraction of phenolic compounds using two different sonotrodes was validated. The lyophilized extracts from AC-p, MD-p, and SP-p were found to contain various phenolic compounds belonging to proanthocyanidins, flavonols, anthocyanins, flavan-3-ols, flavone, hydroxycinnamic acids, and hydroxybenzoic acids, which might be responsible for the demonstrated antioxidant capacities against synthetic free radicals (DPPH and ABTS), biological free radicals (peroxyl radicals, as assessed by the ORAC assay) and superoxide anions (as evaluated by the photoluminescence assay).

CRediT authorship contribution statement

Luis Condezo-Hoyos: Writing – review & editing, Writing – original draft, Visualization, Supervision, Software, Resources, Project administration, Methodology, Investigation, Funding acquisition, Formal analysis, Conceptualization. **Narda Velasco-Salazar:** Writing – original draft, Visualization, Software, Methodology, Investigation, Formal analysis, Data curation. **Lilian Toribio-Lopez:** Visualization, Methodology, Investigation, Formal analysis, Data curation. **Paola Cortés-Avendaño:** Validation, Software, Methodology, Formal analysis, Data curation. **Julio Vidaurre-Ruiz:** Validation, Software, Methodology, Formal analysis, Data curation. **Paulo Torres-Mayanga:** Validation, Methodology, Formal analysis, Data curation. **Jukka-Pekka Suomela:** Writing – review & editing, Supervision. **Baoru Yang:** Writing – review & editing, Supervision. **Ye Tian:** Writing – review & editing, Writing – original draft, Visualization, Methodology, Investigation, Data curation.

Declaration of competing interest

The authors declare that they have no known competing financial interests or personal relationships that could have appeared to influence the work reported in this paper.

Acknowledgement

This research was funded by Consejo Nacional de Ciencia, Tecnología e Innovacion from ProCIENCIA (CONCYTEC, Peru), Project PE501083020-2023 “Inulinas multifenólicas como prebióticos personalizados moduladores de la composición y la actividad de la microbiota intestinal en obesidad obtenidas mediante la tecnología verde de ultrasonidos multifrecuencia intermedia a partir de compuestos fenólicos puros y extractos fenólicos de residuos de frutas tropicales y andinas”. This joint research was also supported by the Research Council of Finland’s Academy Research Fellowship (PhenolLAB project, Decision No. 362319), the Research Council of Finland’s research infrastructure funding (Decision No. 337980), and the European Union-Next Generation EU instrument funding (RRF) for the FOODNUTRI National Infrastructure Network (Decision No. 345916). The authors of the Innovative Technology, Food and Health Research Group (ITFH) thank Dr. Américo Guevara Perez for the support received in the modernization of the scientific infrastructure of the “Instituto de Investigación de Bioquímica y Biología Molecular” (IIBBM), which demonstrated his vision for the future in consolidating scientific activity at “Universidad Nacional Agraria La Molina” (UNALM).

Appendix A. Supplementary data

Supplementary data to this article can be found online at https://doi.org/10.1016/j.fbio.2026.108934.

Data availability

Data will be made available on request.

References

Aguilar-Hernandez, G., Garcia-Magana, M. L., Vivar-Vera, M. L. A., Sayago-Ayerdi, S. G., Sanchez-Burgos, J. A., Morales-Castro, J., Anaya-Esparza, L. M., & Montalvo Gonzalez, E. (2019). Optimization of ultrasound-assisted extraction of phenolic compounds from Annona muricata By-Products and pulp. *Molecules, 24*(5).

Aguilar-Hernández, G., García-Magaña, M.d. L., Vivar-Vera, M.d. l.Á., Sáyago-Ayerdi, S. G., Sánchez-Burgos, J. A., Morales-Castro, J., Anaya-Esparza, L. M., & Montalvo González, E. (2019). Optimization of ultrasound-assisted extraction of phenolic compounds from Annona muricata By-Products and pulp. *24*(5), 904.

Ahmad, T., Esposito, F., & Cirillo, T. (2024). Valorization of agro-food by-products: Advancing sustainability and sustainable development goals 2030 through functional compounds recovery. *Food Bioscience, 62*.

Almeida, J.d. S. O.d., Dias, C. O., Arriola, N. D. A., de Freitas, B. S. M., de Francisco, A., Petkowicz, C. L. O., Araujo, L., Guerra, M. P., Nodari, R. O., & Amboni, R. D. M. C. (2020). Feijoa (Acca sellowiana) peel flours: A source of dietary fibers and bioactive compounds. *Food Bioscience, 38*.

Areti, H. A., Muleta, M. D., Abo, L. D., Hamda, A. S., Adugna, A. A., Edae, I. T., Daba, B. J., & Gudeta, R. L. (2024). Innovative uses of agricultural by-products in the food and beverage sector: A review. *Food Chemistry Advances, 5*.

Avdović, E., Antonijević, M., Simijonović, D., Grujović, M., Marković, K., Milenković, D., Ćirić, A., & Marković, Z. (2025). Ultrasound-assisted extraction of bioactive phenolics from Marselan and Shiraz grape skins: A step toward circular economy in food and pharmaceutical industry. *LWT, 224*.

Bampouli, A., Goris, Q., Hussain, M. N., Louisnard, O., Stefanidis, G. D., & Van Gerven, T. (2024). Importance of design and operating parameters in a sonication system for viscous solutions: Effects of input power, horn tip diameter and reactor capacity. *Chemical Engineering and Processing - Process Intensification, 198*.

Bello, U., Adamu, H., Amran, N. A., & Qamar, M. (2025). Green extraction technologies: Process systems, techno-economic and lifecycle analyses. *Cleaner Engineering and Technology*.

Biswal, R. P., Patnana, D. P., & Vutukuri, V. N. R. K. (2022). Metabolic profiling of Averrhoa carambola fruit extract using UHPLC-ESI-QTOF-MS and determination of the concentration of essential elements using MP-AES. *Analytical Chemistry Letters, 12*(4), 505–527.

Boateng, I. D., & Clark, K. (2024). Trends in extracting Agro-byproducts' phenolics using non-thermal technologies and their combinative effect: Mechanisms, potentials, drawbacks, and safety evaluation. *Food Chemistry, 437*(Pt 1), Article 137841.

Brysev, A. P., Klopotov, R. V., & Makalkin, D. I. (2019). Ultrasound ablation of a solid sample in water accompanied by formation of nanoparticles. *Physics of Wave Phenomena, 27*(1), 51–55.

Cano-Lamadrid, M., Martínez-Zamora, L., Castillejo, N., Bueso, M. C., Kessler, M., & Artés-Hernández, F. (2023). Ultrasound-assisted ethanolic extraction of punicalagin from pomegranate by-products influenced by cultivar, pre-drying treatment, particle size, and temperature. *LWT, 186*.

Carciochi, R. A., D'Alessandro, L. G., Vauchel, P., Rodriguez, M. M., Nolasco, S. M., & Dimitrov, K. (2017). Valorization of agrifood By-Products by extracting valuable bioactive compounds using green processes. In *Ingredients extraction by physicochemical methods in food* (pp. 191–228).

Chan, C. H., See, T. Y., Yusoff, R., Ngoh, G. C., & Kow, K. W. (2017). Extraction of bioactives from Orthosiphon stamineus using microwave and ultrasound-assisted techniques: Process optimization and scale up. *Food Chemistry, 221*, 1382–1387.

Chau, C., Chienb, P., & Chen, C. (2005). Influence of insoluble fiber fractions from carambola and carrot on intestinal enzymes and fecal bacterial enzymes in hamsters. *Nutrition Research, 25*, 947–957.

Conceicao, N., Albuquerque, B. R., Pereira, C., Correa, R. C. G., Lopes, C. B., Calhelha, R. C., Alves, M. J., Barros, L., & I, C. F. R. F. (2019). By-Products of camu-camu [Myrciaria dubia (Kunth) McVaugh] as promising sources of bioactive high added-value food ingredients: Functionalization of yogurts. *Molecules, 25*(1).

Condezo-Hoyos, L., Cortes-Avendano, P., Lama-Quispe, S., Calizaya-Milla, Y. E., Mendez-Albinana, P., & Villamiel, M. (2024). Structural, chemical and technofunctional properties pectin modification by green and novel intermediate frequency ultrasound procedure. *Ultrasonics Sonochemistry, 102*, Article 106743.

Cortés-Avendaño, P., Quispe-Roque, J., Macavilca, E. A., & Condezo-Hoyos, L. (2024). High methoxyl pectin grafted onto gallic acid by one- and two-pot redox-pair procedures. *Food Chemistry, 455*, Article 139865.

Cruz, J. M.d. A., Corrêa, R. F., Sanches, E. A., Campelo, P. H., & Bezerra, J.d. A. (2024). Amazonian fruits: A systematic review of the literature and critical analysis of its trends. *Food Bioscience, 62*.

Cuna, E. C. E. (2018). EVALUATION AND CHARACTERIZATION OF THE BIOACTIVE COMPOUNDS OF CAMU-CAMU [Myrciaria dubia (H.B.K.) Mc Vaug. In *Biblioteca da Faculdade de Engenharia de Alimentos, 128*. Sao Paulo. Brasil: Universidade Estadual de Campinas.

da Silva, L. A., Scapim, M. R.d. S., da Silva, J. F., Stafussa, A. P., Aranha, A. C. R., Jorge, L. M.d. M., Defendi, R. O., Júnior, O.d. O. S., & Madrona, G. S. (2023). Modeling the extraction of bioactive compounds of green and red camu-camu peel and identification using UPLC-MS/MS. *Chemical Engineering Research and Design, 196*, 1–12.

Duymus, H. G., Goger, F., & Baser, K. H. (2014). In vitro antioxidant properties and anthocyanin compositions of elderberry extracts. *Food Chemistry, 155*, 112–119.

Ebrahimi, S. L., Khosravi-Nikou, M. R., & Hashemabadi, S. H. (2018). Sonoreactor optimization for ultrasound assisted oxidative desulfurization of liquid hydrocarbon. *Petroleum Science and Technology, 36*(13), 959–965.

Egues, I., Hernandez-Ramos, F., Rivilla, I., & Labidi, J. (2021). Optimization of ultrasound assisted extraction of bioactive compounds from apple pomace. *Molecules, 26*(13).

Esteban-Lustres, R., Sanz, V., Domínguez, H., & Torres, M. D. (2022). Ultrasound-assisted extraction of high-value fractions from fruit industrial processing waste. *11*(14), 2089.

Exposito-Almellon, X., Munguia-Ubierna, A., Duque-Soto, C., Borras-Linares, I., Quirantes-Pine, R., & Lozano-Sanchez, J. (2025). Optimized ultrasound-assisted extraction for enhanced recovery of valuable phenolic compounds from olive By-Products. *Antioxidants, 14*(8).

Foujdar, R., Bera, M. B., & Chopra, H. K. (2020). Optimization of process variables of probe ultrasonic-assisted extraction of phenolic compounds from the peel of Punica granatum Var. Bhagwa and it's chemical and bioactivity characterization. *44*(1), Article e14317.

Fracassetti, D., Costa, C. L. M., & Tomás-Barberán, F. A. (2013). Ellagic acid derivatives, ellagitannins, proanthocyanidins and other phenolics, vitamin C and antioxidant capacity of two powder products from camu-camu fruit (Myrciaria dubia). *Food Chemistry, 139*, 578–588.

Ganoza-Yupanqui, M. L., Muñoz-Acevedo, A., Ybañez-Julca, R. O., Mantilla-Rodriguez, E., Zavala, E., Gajardo, S., Ríos, M., Benites, J., & Martinez, J. L. (2021). Potential antioxidant effect of fruit peels for human use from northern Peru, compared by 5 different methods. *Boletin Latinoamericano y del Caribe de Plantas Medicinales y Aromaticas, 20*(6), 611–637.

Gil-Martin, E., Forbes-Hernandez, T., Romero, A., Cianciosi, D., Giampieri, F., & Battino, M. (2022). Influence of the extraction method on the recovery of bioactive phenolic compounds from food industry by-products. *Food Chemistry, 378*, Article 131918.

Gogate, P. R., Sutkar, V. S., & Pandit, A. B. (2011). Sonochemical reactors: Important design and scale up considerations with a special emphasis on heterogeneous systems. *Chemical Engineering Journal, 166*(3), 1066–1082.

Hielscher, K. (2012). Ultrasonic milling and dispersing technology for nano-particles. *MRS Online Proceedings Library, 1479*(1), 21–26.

Hu, J., Ma, L., Liu, X., Li, H., Zhang, M., Jiang, Z., & Hou, J. (2022). Superfine grinding pretreatment enhances emulsifying, gel properties and in vitro digestibility of laccase-treated α-Lactalbumin. *LWT, 157*.

Huo, D., Dai, J., Yuan, S., Cheng, X., Pan, Y., Wang, L., & Wang, R. (2023). Eco-friendly simultaneous extraction of pectins and phenolics from passion fruit (Passiflora edulis Sims) peel: Process optimization, physicochemical properties, and antioxidant activity. *International Journal of Biological Macromolecules, 243*, Article 125229.

Islam, S., Alam, M. B., Ahmed, A., Lee, S., Lee, S. H., & Kim, S. (2020). Identification of secondary metabolites in Averrhoa carambola L. bark by high-resolution mass spectrometry and evaluation for alpha-glucosidase, tyrosinase, elastase, and antioxidant potential. *Food Chemistry, 332*, Article 127377.

İşman, N., Sıcak, Y., & Terzioğlu, P. (2025). Polyvinyl alcohol/chitosan composite films with pomegranate peel powder: Improved bioactivity and biodegradability. *Materials Today Communications, 48*.

Kiselova-Kaneva, Y., Galunska, B., Nikolova, M., Dincheva, I., & Badjakov, I. (2022). High resolution LC-MS/MS characterization of polyphenolic composition and evaluation of antioxidant activity of Sambucus ebulus fruit tea traditionally used in Bulgaria as a functional food. *Food Chemistry, 367*, Article 130759.

Kobus, Z., Buczaj, A., Pecyna, A., Kapica, J., Findura, P., & Kocira, S. (2023). Application of response surface method in pulsed ultrasound-assisted extraction of complex plant materials—A case study on Cannabis sativa L. *Applied Sciences, 13*, 760.

Krzywicka, M., & Kobus, Z. (2023). Effect of the shape of ultrasonic vessels on the chemical properties of extracts from the fruit of Sorbus aucuparia. *Applied Sciences, 13*(13).

Kumar, K., Srivastav, S., & Sharanagat, V. S. (2021). Ultrasound assisted extraction (UAE) of bioactive compounds from fruit and vegetable processing by-products: A review. *Ultrasonics Sonochemistry, 70*, Article 105325.

Lin, L. Z., Sun, J., Chen, P., Monagas, M. J., & Harnly, J. M. (2014). UHPLC-PDA-ESI/HRMSn profiling method to identify and quantify oligomeric proanthocyanidins in plant products. *Journal of Agricultural and Food Chemistry, 62*(39), 9387–9400.

Liu, Y., Wang, L., Liu, F., & Pan, S. (2016). Effect of grinding methods on structural, physicochemical, and functional properties of insoluble dietary fiber from Orange peel. *2016*(1), Article 6269302.

López, G. G., Brousse, M. M., & Linares, A. R. (2023). Kinetic modelling of total phenolic compounds from Ilex paraguariensis (St. Hil.) leaves: Conventional and ultrasound assisted extraction. *Food and Bioproducts Processing, 139*, 75–88.

Magalhaes, L. M., Santos, F., Segundo, M. A., Reis, S., & Lima, J. L. (2010). Rapid microplate high-throughput methodology for assessment of Folin-Ciocalteu reducing capacity. *Talanta, 83*(2), 441–447.

Mandrone, M., Lorenzi, B., Maggio, A., La Mantia, T., Scordino, M., Bruno, M., & Poli, F. (2014). Polyphenols pattern and correlation with antioxidant activities of berries extracts from four different populations of Sicilian Sambucus nigra L. *Natural Product Research, 28*(16), 1246–1253.

Matsusaka, Y., & Kawabata, J. (2010). Evaluation of antioxidant capacity of non-edible parts of some selected tropical fruits. *Food Science and Technology Research, 16*(5), 467–472.

Medina, M. B. (2011). Determination of the total phenolics in juices and superfruits by a novel chemical method. *Journal of Functional Foods, 3*(2), 79–87.

Nanzai, B., Okitsu, K., Takenaka, N., Bandow, H., Tajima, N., & Maeda, Y. (2009). Effect of reaction vessel diameter on sonochemical efficiency and cavitation dynamics. *Ultrasonics Sonochemistry, 16*(1), 163–168.

Natolino, A., & Celotti, E. (2022). Ultrasound treatment of red wine: Effect on polyphenols, mathematical modeling, and scale-up considerations. *LWT, 154*.

Noor, A., Moyle, P. M., Malik, A., Ziora, Z. M., & Pant, K. K. (2024). Transformative upcycling of fruit-vegetable waste for nutraceutical and pharmaceutical breakthroughs and circular economy evolution. *Process Safety and Environmental Protection, 187*, 1022–1036.

Ou, B., Chang, T., Huang, D., & Prior, R. L. (2019). Determination of total antioxidant capacity by Oxygen Radical Absorbance Capacity (ORAC) using fluorescein as the fluorescence probe: First action 2012.23. *Journal of AOAC International, 96*(6), 1372–1376.

Pandey, A. K., Thakur, S., Mehra, R., Kaler, R. S. S., Paul, M., & Kumar, A. (2025). Transforming Agri-food waste: Innovative pathways toward a zero-waste circular economy. *Food Chemistry X, 28*, Article 102604.

Pangestu, N. P., Miyagusuku-Cruzado, G., & Giusti, M. M. (2020). Copigmentation with chlorogenic and ferulic acid affected color and anthocyanin stability in model beverages colored with Sambucus peruviana, Sambucus nigra, and Daucus carota during storage. *Foods, 9*(10).

Pantaleón-Velasco, M.d. R., Ruiz-López, I. I., Pérez-Silva, A., Bravo-Clemente, L., Mateos, R., Ruiz-Espinosa, H., & Vivar-Vera, M.d. l. A. (2014). Antioxidant and functional properties of a high dietary fibre powder from carambola (Averrhoa carambola L.) pomace. *49*(9), 2101–2110.

Papoutsis, K., Pristijono, P., Golding, J. B., Stathopoulos, C. E., Bowyer, M. C., Scarlett, C. J., & Vuong, Q. V. (2018). Screening the effect of four ultrasound-assisted extraction parameters on hesperidin and phenolic acid content of aqueous citrus pomace extracts. *Food Bioscience, 21*, 20–26.

Patist, A., & Bates, D. (2011). Industrial applications of high power ultrasonics. In H. Feng, G. Barbosa-Canovas, & J. Weiss (Eds.), *Ultrasound technologies for food and bioprocessing* (pp. 599–616). New York, NY: Springer New York.

Piasecka, I., Górska, A., Kalisz, S., Brzezińska, R., & Wiktor, A. (2022). Ultrasound-assisted extraction of bioactive compounds from black currant and chokeberry pomaces. *The 3rd International Electronic Conference on Foods: Food, Microbiome, and Health—A Celebration of the 10th Anniversary of Foods' Impact on Our Wellbeing)*.

Pimenta da Silva, O. L., Lira de Moura, H., Flores Trindade, M. E., Shirota Imada, K., Mota de Souza Lima, I., & Junger Teodoro, A. (2023). PRODUCTION AND CHARACTERIZATION OF BIOACTIVE EXTRACT OF CAMU-CAMU (Myrciaria dubia). *South American Journal of Basic Education, Technical and Technological, 10*(2), 6.

Popov, I., & Lewin, G. (2005). Photochemiluminescent detection of antiradical activity. VII. Comparison with a modified method of thermo-initiated free radical generation with chemiluminescent detection. *Luminescence, 20*(4-5), 321–325.

Porras-Mija, I., Chirinos, R., García-Ríos, D., Aguilar-Galvez, A., Huaman-Alvino, C., Pedreschi, R., & Campos, D. (2020). Physico-chemical characterization, metabolomic profile and in vitro antioxidant, antihypertensive, antiobesity and antidiabetic properties of Andean elderberry (Sambucus nigra subsp. peruviana). *Journal of Berry Research, 10*(2), 193–208.

Qin, X., Dong, X., Tang, J., Chen, Y., Xie, J., Cheng, Y., Zheng, B., Hu, X., & Yu, Q. (2023). Comparative analysis of dietary fibers from grapefruit peel prepared by ultrafine grinding: Structural properties, adsorption capacities, *in vitro* prebiotic activities. *Food Bioscience, 56*.

Rojas-Lima, J. E., Domínguez-Pacheco, A., Hernández-Aguilar, C., Hernández-Simón, L. M., & Cruz-Orea, A. (2021). Statistical methods for the analysis of thermal images obtained from corn seeds. *SN Applied Sciences, 3*(4).

Rojas-Ocampo, E., Torrejon-Valqui, L., Munoz-Astecker, L. D., Medina-Mendoza, M., Mori-Mestanza, D., & Castro-Alayo, E. M. (2021). Antioxidant capacity, total phenolic content and phenolic compounds of pulp and bagasse of four Peruvian berries. *Heliyon, 7*(8), Article e07787.

Rush, M. D., Rue, E. A., Wong, A., Kowalski, P., Glinski, J. A., & van Breemen, R. B. (2018). Rapid determination of procyanidins using MALDI-ToF/ToF mass spectrometry. *Journal of Agricultural and Food Chemistry, 66*(43), 11355–11361.

Santos, K. C., Guedes, J. S., Rojas, M. L., Carvalho, G. R., & Augusto, P. E. D. (2021). Enhancing carrot convective drying by combining ethanol and ultrasound as pre-treatments: Effect on product structure, quality, energy consumption, drying and rehydration kinetics. *Ultrasonics Sonochemistry, 70*, Article 105304.

Shahbaz, M., Riaz, M., Momal, U., Rasool, I. F. U., Naeem, H., Raza, N., Moreno, A., Khalid, W., & Esatbeyoglu, T. (2025). Green solvent extraction and eco-friendly novel techniques of bioactive compounds from plant waste: Applications, future perspective and circular economy. *Applied Food Research, 5*(2).

Sharayei, P., Azarpazhooh, E., Zomorodi, S., & Ramaswamy, H. S. (2019). Ultrasound assisted extraction of bioactive compounds from pomegranate (Punica granatum L.) peel. *LWT, 101*, 342–350.

Sidor, A., & Gramza-Michałowska, A. (2015). Advanced research on the antioxidant and health benefit of elderberry (Sambucus nigra) in food – A review. *Journal of Functional Foods, 18*, 941–958.

Tian, Y., Laaksonen, O., Haikonen, H., Vanag, A., Ejaz, H., Linderborg, K., Karhu, S., & Yang, B. (2019). Compositional diversity among blackcurrant (Ribes nigrum) cultivars originating from European countries. *Journal of Agricultural and Food Chemistry, 67*(19), 5621–5633.

Tian, Y., Liimatainen, J., Alanne, A. L., Lindstedt, A., Liu, P., Sinkkonen, J., Kallio, H., & Yang, B. (2017). Phenolic compounds extracted by acidic aqueous ethanol from berries and leaves of different berry plants. *Food Chemistry, 220*, 266–281.

Ulusoy, U., & Yekeler, M. (2014). Dynamic image analysis of calcite particles created by different mills. *International Journal of Mineral Processing, 133*, 83–90.

Uzlasir, T., Kadiroglu, P., Selli, S., & Kelebek, H. (2020). LC-DAD-ESI-MS/MS characterization of elderberry flower (Sambucus nigra) phenolic compounds in ethanol, methanol, and aqueous extracts. *Journal of Food Processing and Preservation, 45*(8).

Voß, J., & Wittkowski, R. (2023). Acoustic propulsion of nano- and microcones: Dependence on particle size, acoustic energy density, and sound frequency. Arxiv Con-mat. Cornell Univertivy *arXiv preprint arXiv:2307.00681*, 1–19.

Yi, M., Shen, Z., Zhang, X., & Ma, S. (2012). Vessel diameter and liquid height dependent sonication-assisted production of few-layer graphene. *Journal of Materials Science, 47*(23), 8234–8244.